Geochemical identification of particulate lead pollution in shallow groundwater and estimation of lead contents in airborne pollutants in inhabited areas in Kabwe, Zambia

Kazuhiro TOYODA[1,2]*, Shota NAKANO[1], Shunitz TANAKA[1,2], Kawawa BANDA[3], Imasiku A. NYAMBE[3], Tsuyoshi ISHIKAWA[4], Shouta NAKAYAMA[5], Mayumi ISHIZUKA[5]

[1] Graduate School of Environmental Science, Hokkaido University, Japan
[2] Faculty of Environmental Earth Science (FEES), Hokkaido University, Japan
[3] Integrated Water Resources Management Centre, Department of Geology, School of Mines, The University of Zambia, Zambia
[4] Kochi Institute for Core Sample Research, Japan Agency for Marine-Earth Science and Technology (JAMSTEC), Japan
[5] Graduate School of Veterinary Medicine, Hokkaido University, Japan

*: Corresponding author; Email address: kazuhiro@ees.hokudai.ac.jp (K.Toyoda); Postal address: Graduate School of Environmental Science, Hokkaido University, N10W5, kita-ku, Sapporo 060-0810, JAPAN

To be submitted to *Applied Geochemistry*.

August 29th, 2021

Keywords: Shallow groundwater, Lead particulate, Mining pollution, Lead isotopes, Airborne dust, Cerium anomaly

Abstract

The town of Kabwe has been exposed to the most severe lead pollution due to mining activities in the 20th century. A large tailing (slag) hill containing over 1% of Pb is still standing within the mine's licensed area. We analysed the chemical composition and lead isotope ratios in seventeen shallow wells, five deep wells in the inhabitants' area, three ponds and three borehole wells in the area of the mine, and in the surrounding areas, we examined two samples from the soil's surface and nineteen 1-m deep core samples at each of the 15 sites. We found low dissolved Pb (<0.04 µg/L) but high particulate Pb concentrations (2–100 µg/L) in seventeen shallow groundwater samples. Five of the shallow wells exceeded the World Health Organization (WHO) guideline (10 µg/L) for total-Pb concentration. However, three of the five shallow wells had low dissolved Zn and sulphate ion concentrations (<1 µg/L; <50mg/L), suggesting a low amount of Pb transfers through the aquifer. The isotopic water and soil samples data clarified that the Pb pollution in the shallow groundwaters is derived from the tailings deposit.

Most of the shallow groundwater samples had a negative cerium (Ce) anomaly in the rare earth element (REE) pattern, indicating contributions from the dolomite aquifer in this area. However, the positive correlation between Pb/Ce and Pb/Al ratios in the particulates exhibited that the lead pollutants were derived from the aluminosilicates on the land. The estimated Pb contents in particulates in the shallow-well water distributed geographically was similar to the Pb bulk concentration contour map of the surface soil. However, we found a significant fractionation between them e.g. the Pb level in the particulates in the well water taken from several wells in the mine's zone (0.12–0.2 % of Pb in soil) was estimated ats ca. 0.5%. Furthermore, the analysis of the grain-size fractions in a 2-km transect soil demonstrated that Pb was eight times enriched in the silt fraction (<53 µm) than a very coarse sand fraction (1–2 mm). Therefore, we concluded that the particulates in the well water were mainly derived from the aeolian dust (>0.45 µm) at the well site during the last days before the sampling. These results provide some guidelines for reducing health hazards of the inhabitants and suggest that chemical analysis in well water may be a resourceful methodology for chemical analysis of dust in the air.

1. Introduction

Mining and ore processing generate a large amount of metal-rich dust, and the fallout produces soil pollution (e.g. Csavina et al., 2012; Ettler, 2015). Additionally, the remaining tailings deposit became a source of water pollution (e.g. Kossoff et al., 2014; Uddh Söderberg et al., 2019; Walraven et al., 2014). With growing global demands for freshwater sources, shallow groundwater is still essential as a local water source in many areas but is vulnerable to anthropogenic contaminations. Although it was believed that only the soluble phases could facilitate the transport of pollutants through an aquifer, the possibility of colloid-bound transport of contaminants in groundwater was also highlighted three decades ago (Corapcioglu and Jiang, 1993). Rare earth elements (REEs) in groundwater are used as a 'fingerprinting" tool to determine possible sources, the mixing of different sources, and elucidate groundwater flow paths (Johannesson, 2006). Lead stable isotope ratios in groundwater are also measured to determine possible sources of lead pollution, the mixing and the flow paths. However, under some criteria, the Pb isotope composition of the primary source of Pb must be relatively homogeneous, and those of other potential Pb sources in the area could be defined (Faure and Mensing, 2005).

The town of Kabwe in the Republic of Zambia was labelled as one of the ten most polluted places on the Earth (Blacksmith Institute, 2013). Although it prospered as a Pb–Zn mining town in the 20th century (Southwood et al., 2019), the unregulated mining and ore smelting caused the heavy metal-polluted soil in large areas around the mining area (Tembo et al., 2006). A tailings deposit in the mining area remains a continued source of contamination through weathering and erosion after the mine closure in 1994 (Bose-O'Reilly et al., 2018; Kříbek et al., 2019; Nakayama et al., 2011, 2013, 2019). Inorganic Pb can be absorbed in the human body mainly by oral and respiratory exposures. One of the primary concerns about Pb toxicity during the development of the nervous system in children is the potential to affect intelligence (e.g. Wolfe et al., 2016). Many animal studies have already been performed on monitoring pollution and simulating Pb toxicity (Kataba et al., 2021; Nakata et al., 2021a). Yabe et al. (2015, 2018) demonstrated that the lead levels in the children's blood continue to be elevated even after mine closure; lead toxicity remains a critical issue for the local people (Nakata et al., 2021b; Yohannes et al., 2020, 2021). Ettler et al. (2020) reported the mineralogy and oral bio-accessibility of the dust component at the slag deposit. The

fine-grain particulate matter (PMs) has received considerable attention in recent years (Dockery et al., 1993), but the heavy metal concentration in airborne dust remains unknown in this area since it takes a lot of time and effort to quantify the heavy metal concentration and amount in airborne dust (e.g. Aničić et al., 2012; Ghorbel et al., 2014).

In Kabwe, shallow groundwater forms an essential source of the potable water supply for many communities in low-cost housing areas; piped connections with local tap water from deep groundwater boreholes are unavailable. Previous studies indicate that the lead levels in the shallow wells were generally below or within the range of the WHO guidelines (10 µg/L) during the summer of 2004 (ZCCM-IH, 2004) and in March 2012 (Phiri, 2016). Nevertheless, the total (dissolved + particulate) Pb concentrations in one-third of the water samples were slightly above the WHO level at that time of the study (ZCCM-IH, 2004). Furthermore, an organic contaminants study of the groundwater (Sorensen et al., 2015) indicates that the mobile compound migrates rapidly from the surface to the shallow groundwater aquifer following the heavy seasonal rains.

In this study, we analysed the chemical composition, including REEs and lead isotope ratios in unfiltered and filtered domestic water from seventeen shallow wells in the inhabited area around the Kabwe abandoned mine. To determine the source and channel of the Pb contamination in the groundwaters within the area of the mine, we analysed samples from the following for comparison: three ponds, three borehole wells, and five deep groundwater samples. The lead isotopic ratios in the silicate fraction of nineteen 1-m deep soil samples were analysed as an analogue of the isotopic ratios in the permeable layers in this area. In addition, chemical and isotopic analyses of grain-size fractions in two of the surface soil samples were examined to determine the chemical composition of the dust in this area. These results permitted us to examine the hypothesis that the Pb pollution may be caused by the contamination of a small amount of dust from the atmosphere. The achievement of this study lies in the estimation of the Pb concentration of dust at the well sites in the inhabited area; we assume that the shallow well is a natural trap of airborne fine-grain PMs.

[Fig. 1]

Fig. 1 (a) Map of the town of Kabwein Zambia, central Africa; (b) Sampling locations of water and soil samples with the Pb content contour in topsoil (modified from Kříbek et al., 2019); (c) Geological map: magnification of the square area in Fig. 1b.

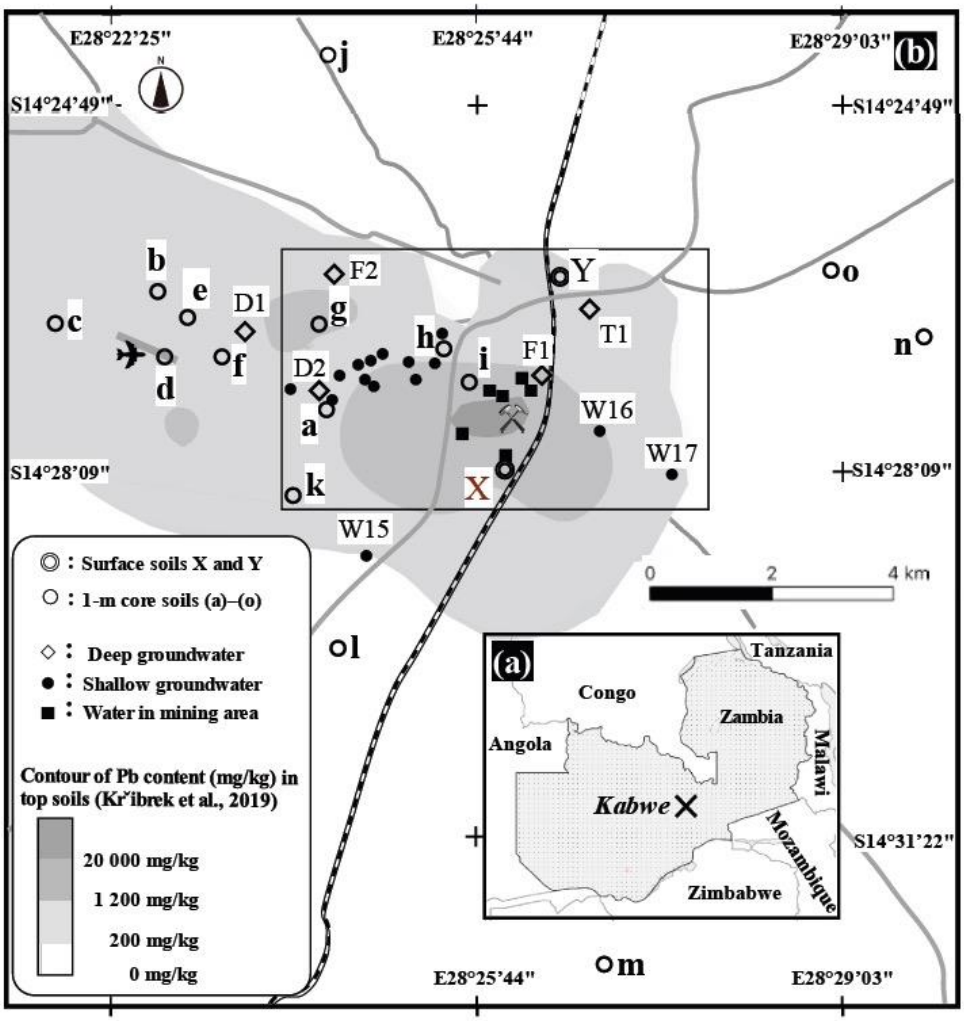
E28°22'25"
E28°25'44"
E28°29'03"
(b)
S14°24'49"
S14°28'09"
S14°31'22"
F2
D1
D2
F1
T1
W15
W16
W17
X
Y
: Surface soils X and Y
: 1-m core soils (a)–(o)
: Deep groundwater
: Shallow groundwater
: Water in mining area
Contour of Pb content (mg/kg) in top soils (Kříbrek et al., 2019)
20 000 mg/kg
1 200 mg/kg
200 mg/kg
0 mg/kg
0 2 4 km
(a)
Tanzania
Congo
Zambia
Angola
Malawi
Kabwe
Mozambique
Zimbabwe

100

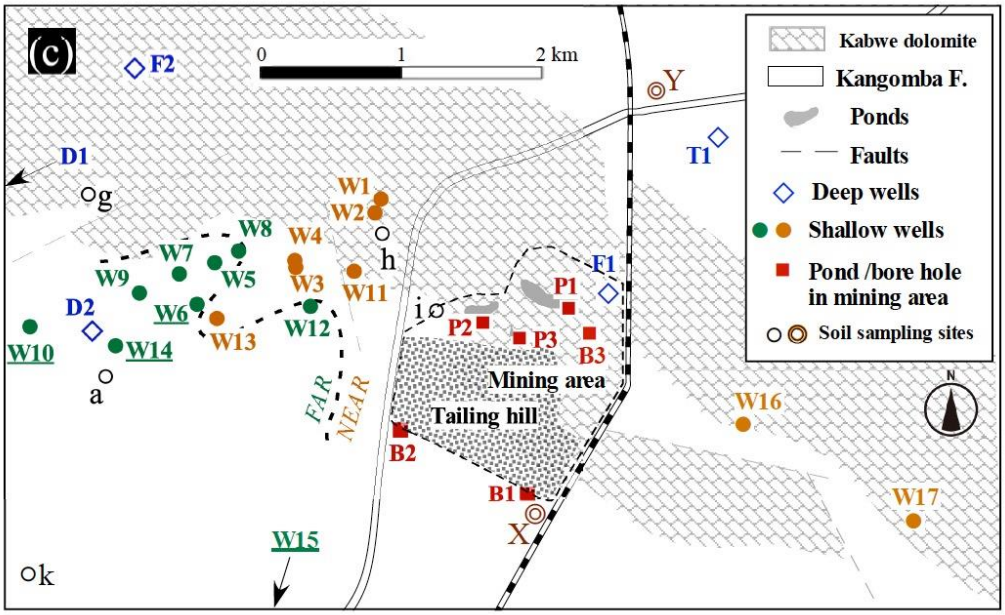
(c)
F2
0 1 2 km
D1
W1
W2
W8
W4
W7
W9
W5
W3
W11
D2
W6
W12
W13
W10
W14
F1
P1
P2
P3
B3
Mining area
Tailing hill
FAR
NEAR
B2
B1
W15
W16
W17
Y
T1
X
Kabwe dolomite
Kangomba F.
Ponds
Faults
Deep wells
Shallow wells
Pond /bore hole in mining area
Soil sampling sites

101

2. SAMPLES AND ANALYTICAL PROCEDURE

2.1 Geological setting

The town of Kabwe resides on a plateau in central Zambia, a landlocked country in southern Africa (Fig. 1a). The large-scaled carbonate-hosted Pb–Zn mine (Kamona and Friedrich, 2007) is located at latitude 14°27'S and longitude 28°26'E in the town of Kabwe (Hammer and pick mark in Fig. 1b). The tailing hill of about one square kilometre (shown as the dotted area in Fig. 1c) is in the mining area (shown as the broken line area in Fig. 1c). The Kabwe abandoned mine occupies a position within a central syncline of massive dolomite. The Kabwe (massive, bedded, and schistose) Dolomite distributes along the NW-SE direction around the mine, overlain by laterite, typically 5–20 m thick (Houston, 1982). The dolomite zone is surrounded by the Kangomba Formation, which mainly consists of schists. The shallow groundwater aquifer units are around 10 m depth, which include the laterite/dolomite and the surrounding schist (W1–17 in Figs. 1b–1c). The deep groundwater (F1–2, D1–2, T1 in Figs. 1b–1c) draws water from the Kabwe Dolomite aquifer at 50–100 m depth in this study. Additionally, the groundwater flow directions are considered concordant with the topographic surface and the predominantly trended NW-SE (ZCCM-IH, 2004).

Fig. 1b shows the contour map of the Pb concentration of topsoil in the abbreviated form from the map by (Kříbek et al., 2019). The general information about soil contamination was also reviewed by (Nakayama et al., 2011). The most condensed hatched area in Fig. 1b indicates that the highest Pb concentration (>2%: >20 000 mg/kg) at the tailings deposit and the vicinity where three small ponds are located (P1–P3 in Fig. 1c). The Pb distribution (>200 mg/kg) extends from the mining area downwind, WNW of Kabwe. This trend is mainly due to gentle east winds annually prevailing in the area and partly due to the distribution of dolomite. The monthly average wind velocities during the rainless period (June–September) are 4.2–5.4 m/s, and the annual precipitation is ca. 910 mm in the town of Kabwe (Cedar Lake Ventures, 2020). A company (Sable Zinc Kabwe Limited) has undertaken groundwater level and quality monitoring of the boreholes (e.g. B1–B3 in Fig. 1c) around the mining area to check the migration of contaminants from the mine into the regional aquifer.

[Table 1]

Table 1. Water sampling sites in Kabwe (July 5-8, 2016) and the dissolved major chemical composition of water filtered by 0.45 μm syringe filter.

Table 1. Water sampling sites (July 5-8, 2016) and the dissolved major chemical composition of water filtered by 0.45 μm syringe filter.

Sample symbol	Strainer depth (m)#	Sampling site			pH$	Major cation and anion concentration (ppm)						
		Elevation (m)*	Latitude	Longutude		Na^+	K^+	Mg^{2+}	Ca^{2+}	Cl^-	NO_3^-	SO_4^{2-}
P1	0	1164	S14°27' 18 64"	E 28°26' 10 06"	8.3	11.7	8.0	62.3	114.9	12.3	4.6	125.9
P2	0	1172	S14°27' 21 23"	E 28°25' 49 64"	8.1	17.0	11.6	85.7	46.8	15.8	0.0	349
P3	0	1169	S14°27' 24 75"	E 28°25' 14 88"	8.1	16.1	11.1	64.3	142.1	13.8	1.8	331
B1	6	1182	S14°27' 33 59"	E 28°26' 19 85"	7.8	12.7	7.3	46.8	83.9	4.7	0.0	152.7
B2	8	1186	S14°27' 44 79"	E 28°25' 30 41"	8.1	32.4	10.6	71.8	68.8	21.3	0.0	177.3
B3	5	1178	S14°27' 23 69"	E 28°26' 14 88"	8.1	9.8	8.8	62.9	108.5	7.6	9.2	161.6
W1	5	1187	S14°26' 52 63"	E 28°25' 25 64"	8.0	25.0	6.7	56.8	73.1	37.4	71.1	21.7
W2	6	1181	S14°26' 56 44"	E 28°26' 05 56"	7.9	21.6	8.5	64.7	58.4	45.1	59.7	40.4
W3	4	1186	S14°27' 08 08"	E 28°25' 05 57"	7.8¥	33.0	15.5	56.6	57.5	38.0	0.0	109.4
W4	3	1180	S14°27' 09 49"	E 28°26' 06 10"	7.9	50.2	10.9	58.1	40.9	32.6	0.0	114.5
W5	8	1189	S14°27' 07 08"	E 28°24' 46 55"	8.1	29.8	8.7	76.2	54.7	17.4	19.4	32.1
W6	10	1183	S14°27' 17 56"	E 28°24' 42 77"	8.0	39.3	7.0	61.4	60.7	26.7	34.5	11.8
W7^	15	1191	S14°27' 10 61"	E 28°24' 38 48"	7.9	22.9	6.1	48.2	26.3	27.0	47.8	33.7
W8	8	1184	S14°27' 05 36"	E 28°24' 52 17"	7.9	20.6	9.7	48.1	9.9	12.2	8.0	18.7
W9	10	1190	S14°27' 14 80"	E 28°24' 28 82"	7.9	25.0	4.6	35.7	53.7	11.8	17.5	7.3
W10	ca.10	1191	S14°27' 22 98"	E 28°24' 03 19"	8.1	15.1	3.2	27.7	37.7	2.2	0.0	12.5
W11	10	1183	S14°27' 09 65"	E 28°23' 19 29"	8.0	24.1	23.3	142.7	94.0	30.5	0.0	451
W12	5	1186	S14°27' 18 08"	E 28°25' 09 49"	8.1	25.6	7.4	55.4	53.8	30.0	33.0	45.5
W13	ca.10	1189	S14°27' 20 69"	E 28°24' 47 37"	7.8	38.2	8.2	70.1	51.2	50.7	69.1	63.6
W14	15	1194	S14°27' 28 80"	E 28°24' 24 00"	6.9	9.7	1.8	1.9	1.2	0.8	0.0	0.6
W15	5	1181	S14°28' 51 76"	E 28°24' 14 24"	7.5	8.8	1.2	6.4	13.1	2.4	0.0	1.9
W16	10	1178	S14°27' 44 52"	E 28°26' 50 92"	8.1	8.4	5.4	47.3	76.6	6.1	6.1	32.6
W17	8	1175	S14°28' 06 11"	E 28°27' 31 31"	7.9	15.1	5.1	42.5	69.5	17.2	16.0	106.2
T1	Tap	1186	S14°26' 38 72"	E 28°26' 43 17"	8.2	10.3	4.8	35.8	34.2	4.1	5.0	4.8
F1	ca. 100	1173	S14°27' 14 82"	E 28°26' 19 57"	8.0	5.8	4.9	41.5	48.1	3.4	8.2	7.8
F2	ca. 100	1180	S14°26' 22 07"	E 28°24' 24 65"	8.2	5.2	5.3	42.0	66.5	3.4	8.5	7.8
D1	ca. 50	1182	S14°26' 53 05"	E 28°23' 35 88"	8.0	8.6	5.3	40.5	32.4	0.9	1.3	4.3
D2	ca. 50	1192	S14°27' 25 01"	E 28°24' 19 59"	8.0	10.5	3.3	23.7	48.7	2.3	0.7	5.1

#: Interview with the owner of the well ; ^: Disinfectant was added into the well a few days before the water sampling; *:

Google earth data

$: Measured indoors on the evening of sampling; ¥: Measurement after returning to Japan.

2.2 Water samples and the chemical analysis

All 28 water samples were collected on July 2016: 17 shallow-well sites (W1–W17) in the peri-urban housing area (Makululu, Kasanda and Chowa); two deep-well sites (D1, D2), two drinking-water processing facilities (F1, F2) from deep aquifers, tap water at a hotel (T1), three observation borehole wells (B1–B3), and three ponds (P1–P3) in the Kabwe mining area. The tap water in the central business district (e.g. sample T1) is supplied from the facilities. The water sample information is listed in Table 1, and the sampling locations are indicated in Figs. 1b–c. We interviewed each well owner to obtain the strainer depth data in Table 1. The owner of the W7 shallow-well testified that officials came to drop some fungicide powder into the well a few days before the sampling day. Nevertheless, the fungicide powder is a bleached powder (calcium hypochlorite), and we speculate that it has a negligible effect on the chemical composition of the well water.

The well-water samples' pH was measured, and each sample was sealed in a sterile brown polypropylene bottle at the sampling sites. Both bottles of the well-water samples were kept in the refrigerator until the following preparation and chemical analysis. The water sample from the first bottle was filtered using 0.45-μm pore size PTFE (polytetrafluoroethylene) micro-syringe filters (As One Co., Japan) in a sterile laboratory in Japan. 1) The filtered water samples were analysed by the ion analyser (TOA-DKK Co., Ltd., Model IA-300) at the Faculty of Environmental Earth Science (FEES) of Hokkaido University for the anion concentration measurement. The remaining filtered water samples were analysed for ICP chemical measurements after acidification by adding a small portion of ultrapure-grade nitric acid (Kanto Chemicals, Japan) to determine the dissolved components of groundwater; 2) The unfiltered water samples, including the suspended particulate components in groundwater, were shacked and also divided into two samples for analysis as noted in the following: i) Five residues (suspended matter) on the conventional membrane filters (PTFE; pore size 0.45 μm) from 30 mL of a water sample (Fig. A.1) were provided for an X-ray diffraction (XRD) analysis to determine the mineral species of the residues, and ii) another solution that was acidified to 1.2 M nitric acid solution by addition of ultrapure-grade 61% nitric acid

(Kanto Chemical Co.), was analysed for ICP after 2-days of heating at 80°C for the chemical determination of the total, which is defined as the sum of the dissolved and particulate components. Since the colloid is identified as particles of 0.1 µm or less, this dissolved component included the colloidal particle components.

The XRD diffraction analysis of the suspended matter on the PTFE filter was determined by Rigaku Smart-Lab diffractometer (Rigaku Co., Japan) at the Open Facility, Global Facility Center, Creative Research Institution, Hokkaido University with the reference intensity ratio (RIR) method (Hillier, 2000). No significant discrepancy was observed in the XRD charts of the two clay standards: IMt-2, illite (Silver Hill Montana, USA; Clay Mineral Society) (CMS, 2005) and JCSS-5101 sericite (Nabeyama, Japan; Clay Science Society of Japan) (Miyawaki et al., 2010). Sericite is the name given to very fine weathered grains or aggregates of muscovite, colourless mica. Illite is a weathered clay mineral of mica, including muscovite, that shows very similar XRD peaks. The RIR analysis of IMt-2 standard shows 91.0 ± 0.9% of illite-1M (card number: 00-029-1496), 4.7 ± 0.5 % of illite-2M2 (00-043-0685), 3.8 ± 0.6% of quartz (01-085-0794) and 0.50 ± 0.06% of zeolite (01-085-9962) from XRD chart of IMt-2, described as illite (85–90%), and quartz (10–15%) in the datasheet (Clay mineral society, 2005). RIR analysis of JCSS-5101 sericite standard indicates muscovite (82.8 ± 1.0%; -2M1: 00-058-2037 and 13.4 ± 1.0%; -2M1: 01-076-0068), quartz (2.6 ± 1.0%; 01-085-0794), and kaolinite-1A (1.17 ± 0.03%; 00-058-2004).

Major cation concentrations in the water sample were measured by ICP-OES (Seiko Co., SPS7700) at the FEES of Hokkaido University. The trace elemental analysis was carried out with an Agilent 8800 triple quadrupole ICP-MS (ICP-QQQ) mass spectrometer, using the helium collision mode at the Open Facility of Hokkaido University. With the ICP-QQQ, we performed the direct measurement of a solution containing less than 0.5 µg/L of the target elements, without any chemical separation of the matrix and the pre-concentration by evaporation, after the dilution of the groundwater samples that were used to adjust the total cation concentration below 50 mg/L in ca. 3% v/v ultrapure HNO_3. A stock multielement standard solution of REEs was prepared from stock solutions (SPEX Certi Prep Co.). The other stock standard solutions containing major cations and heavy metal cations were prepared from each element's 1 mg/ml standard solutions (Kanto Chemical Co.). Data precision and accuracy were checked by analysis of reference materials (JB-1, JLk-1, JSd-2 and JSd-

3; Potts et al., 1992). No systematic error was observed.

[Table 2]

Table 2. The sampling sites (May 3–7, 2018) in Kabwe, depth, Zn and Pb bulk contents, and the Pb isotopic data in the silicate fraction of 1-m long cores (a-o).

Table 2. The sampling sites and depth, Zn and Pb bulk contents and the Pb isotopic data in the silicate fraction of 1-m long cores (**a-o**).

Site symbols	Site locations			Core depth (cm)	Bulk contents		$^{206}Pb/^{207}Pb$			$^{208}Pb/^{206}Pb$		
	Latitude	Longutude	Elevation (m)*		Pb (ppm)	Zn (ppm)	average	±	2SD	average	±	2SD
				45-55	130	280	1.16751	±	0.00002	2.10472	±	0.00003
a	S 14˚27'34"	E 28˚24'20"	1194	55-60	120	80	1.17282	±	0.00002	2.09810	±	0.00003
				80-95	185	71	1.18669	±	0.00002	2.07760	±	0.00003
b	S 14˚26'36"	E 28˚22'46"	1190	98-100	300	1230	1.16049	±	0.00002	2.10554	±	0.00003
c	S 14˚26'49"	E 28˚21'52"	1201	90-95	35	50	1.26009	±	0.00002	1.96953	±	0.00002
d	S 14˚27'05"	E 28˚22'53"	1190	95-100	180	700	1.15367	±	0.00002	2.11530	±	0.00003
e	S 14˚26'46"	E 28˚23'03"	1189	90-95	120	1000	1.15187	±	0.00002	2.11944	±	0.00003
f	S 14˚27'04"	E 28˚23'24"	1193	95-100	40	40	1.23069	±	0.00002	2.00189	±	0.00003
g	S 14˚26'52"	E 28˚24'17"	1191	90-95	250	350	1.15288	±	0.00001	2.11729	±	0.00003
h	S 14˚27'01"	E 28˚25'26"	1185	90-95	340	700	1.14775	±	0.00002	2.12668	±	0.00003
i	S 14˚27'20"	E 28˚25'39"	1187	90-95	280	760	1.15611	±	0.00002	2.11689	±	0.00003
j	S 14˚24'26"	E 28˚24'19"	1195	90-95	52	77	1.22296	±	0.00002	2.02319	±	0.00002
k	S 14˚28'20"	E 28˚24'03	1191	90-95	71	24	1.20728	±	0.00002	2.04186	±	0.00003
l	S 14˚29'44"	E 28˚24'29"	1184	95-100	18	1	1.20159	±	0.00002	2.05292	±	0.00002
m	S 14˚32'30"	E 28˚26'55"	1187	90-95	23	13	1.23220	±	0.00002	2.00769	±	0.00003
				10-15	35	7	1.15507	±	0.00002	2.15421	±	0.00003
n	S 14˚26'53"	E 28˚29'48"	1195	50-55	64	6	1.15924	±	0.00002	2.16606	±	0.00003
				90-95	95	19	1.15799	±	0.00002	2.16506	±	0.00002
o	S 14˚26'18"	E 28˚28'57"	1203	80-85	250	70	1.20087	±	0.00002	2.05884	±	0.00002

*: Google earth data;

2.3 Soil samples and the chemical analysis

Two kinds of soil samples were also studied: 1) Bulk and the grain-size fraction samples from two surface soils (X and Y); 2) 19 soil samples taken from 1-m deep cores (15 sites (a)–(o)). The sampling location and information are described in Fig. 1

and Table 2, respectively. Soil X is a garden soil sample adjacent to the tailing hill, and Soil Y is a residential soil sample obtained 2 km north from the mining area. These X and Y samples were passed through a 2 mm mesh sieve and were dried at 40 degrees for one week. The dry bulk samples were divided into six grain-size fractions (2–1 mm, 1–0.5 mm, 0.5–0.3 mm, 0.3–0.1 mm, 0.1–0.05 mm, below 0.05 mm) through nylon sieves. The lead and zinc concentrations in the bulk and the grain-size fractions of samples X and Y and bulk core samples (sites (a)–(o)) were analysed with the ICP-QQQ following an HF-HNO_3-$HClO_4$ acid-digestion in a clean area. These soil samples were imported under the permit (27Y303, 27Y304, 29Y1704)) of the Minister of Agriculture, Forestry, and Fisheries, in Japan, by the Plant Protection Law.

2.4 Lead isotopic measurements

In this study, two kinds of ICP-MS were used for Pb isotope ratios ($^{206}Pb/^{207}Pb$ and $^{208}Pb/^{206}Pb$) measurements. The ICP-QQQ was used to analyse the unfiltered groundwater samples (only total Pb > 5 µg/L) and the grain-size fractions of samples X and Y. The measurements were corrected for the mass discrimination by the common Pb isotope standard NIST SRM 981, and the short-term precision of the measurements was 0.2 to 0.3%. Repeated analyses of 10 µg/L Pb solution of the NIST SRM 981, digested rock reference samples of JG-2 and JG-3 yielded the average values with 2SE (σ: standard deviation): $^{206}Pb/^{207}Pb$ = 1.0937 ± 0.0027, 1.1886 ± 0.0032 and 1.1798 ± 0.0036; $^{208}Pb/^{206}Pb$ = 2.1681 ± 0.0044, 2.1015 ± 0.0067 and 2.0954 ± 0.0066, respectively. Pb isotopic ratios obtained for JG-2 and JG-3 were consistent with the literature values (e.g. Tanimizu and Ishikawa, 2006).

Another instrument utilised in our experiment is the MC-ICP-MS NEPTUNE (Thermo Fisher Scientific) located at the Kochi Core Center. The observed Pb isotopic ratios were normalised using the $^{205}Tl/^{203}Tl$ ratio of a Tl isotope reference material, NIST SRM 997, added to the sample before the isotopic determination, following the procedure described in Tanimizu and Ishikawa (2006). Recent repeated analyses of the NIST SRM 981 yielded the following results: $^{206}Pb/^{207}Pb$ = 1.093426 ± 0.000008 (2σ); $^{208}Pb/^{206}Pb$ = 2.166205 ± 0.000027 (2σ). No systematic differences between repeated analyses were noted in this study (N = 7). This instrument was used to determine the $^{206}Pb/^{207}Pb$ and $^{208}Pb/^{206}Pb$ in silicate fraction of core samples (sites (a)–(o) in Fig. 1). The core samples were leached by aqua regia at 80°C for three hours, and the silicate

residues were washed out twice by 1-M nitric acid. Then, the residues were digested in PFA beakers (Savillex) using an HF-HNO_3-$HClO_4$ acid (Toyoda and Haraguchi, 1987), followed by the chromatographic extraction of lead from the digested solution using Eichrom pre-packaged Sr resins. The method of the separation procedure follows the modification of Deniel and Pin (2001). All chemical procedures were carried out in sterile benches (class-100) and evaporators. The 18.2 MΩcm water produced by a Milli-Q system (Millipore) in a class-1000 sterile room was used. The total procedural blank of Pb was from 40 to 130 pg, which was negligible in this study. [Fig. 2]

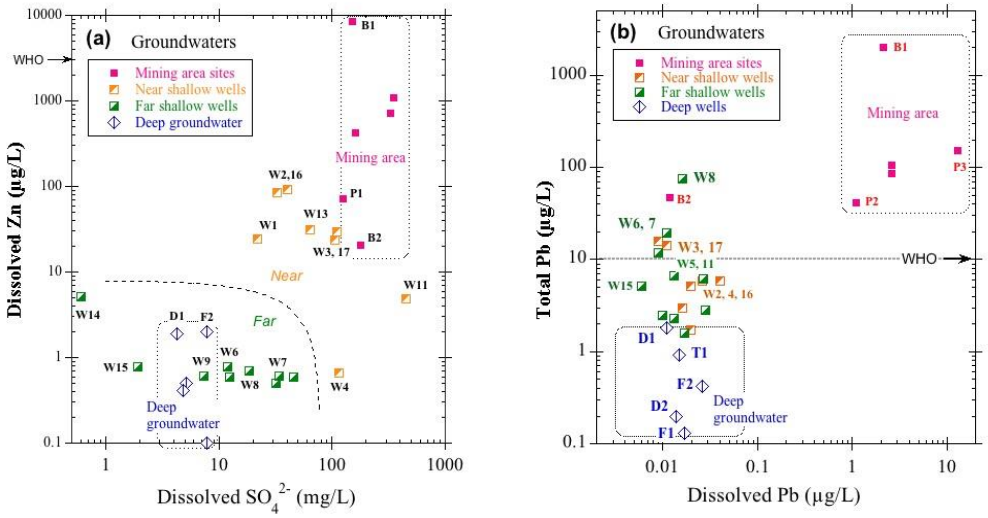

Fig. 2 (a) Dissolved Zn concentration vs sulphate ion concentration; **(b)** Dissolved Pb concentration vs total-Pb concentration in water samples. B: Borehole groundwater; P: Pondwater; W: shallow wells; D: Deep wells; F: water factory; T: Tap water.

Fig. 2 (a) Dissolved Zn concentration vs sulphate ion concentration; (b) Dissolved Pb concentration vs total-Pb concentration in water samples. B: Borehole groundwater; P: Pondwater; W: shallow wells; D: Deep wells; F: water factory; T: Tap water.

3. Results and Discussion

3.1 Chemical composition in groundwaters

Table 1 shows major elemental compositions of 28 filtered (<0.45 µm) water

samples. Most samples were slightly alkaline (pH = 7.8–8.3) and had high Ca and Mg concentrations (high water hardness) due to the dolomite dissolution in this region. The exceptionally soft water samples (W14, W15) were collected from the sites far from the dolomite zone in Fig. 1, indicating that the aquifers of the two samples were throughout the schist layers; therefore, the water samples were free from the dolomite dissolution. The two samples (W14, W15) have also exceptionally low pH, 6.9 and 7.5, respectively, due to the dolomite dissolution. In Table 1, the sulphate ion (SO_4^{2-}) concentrations in the six samples (P1–P3, B1–B3) from the mining area are 126–350 mg/L. This is because of the high concentration induced by the sulphate dissolution followed by the oxidation of the sulphide ore-body (Kamona and Friedrich, 2007). In contrast, the SO_4^{2-} concentrations in the five samples (T1, F1, F2, D1, D2) from the deep aquifers (50–100 m in depth) were low (4–8 mg/L), suggesting that these deep aquifers have been isolated from the tailing influence.

Fig. 2a shows high dissolved Zn^{2+} concentrations (20–10000 µg/L) in the mining area samples and low Zn^{2+} concentrations (0.01–2 µg/L) in the deep-well samples with the same trend of SO_4^{2-} concentrations in these samples. Additionally, these results demonstrate that the shallow-well water samples (W1–W17) are divided explicitly into two groups: the first group having dissolved Zn^{2+} concentrations higher than 20 µg/L or SO_4^{2-} concentrations higher than 100 mg/L, and the second group with low Zn^{2+} and SO_4^{2-} concentration ranges of 0.5–5 µg/L and below 40 µg/L, respectively. In Fig. 1c, the higher concentration group (W1–4, 11, 13, 16, 17) was located in or near the Kabwe Dolomite zone; whereas, the lower concentration group (W5–10, 12, 14, 15) were relatively far from the dolomite zone. In this paper, the two groups are referred to as hydrologically "NEAR" (W1–4, 11, 13, 16, 17) and "FAR" (W5–10, 12, 14, 15) from the shallow-well waters. The geographical boundary is illustrated in Fig. 1c. The hydraulic conductivity values in the Kabwe Dolomite are generally at a greater order of magnitude than the values in schist layers in the Kangomba Formation. The groundwater flows predominantly in NW-SE direction (ZCCM-IH, 2004). Therefore, we can say that the higher values of the dissolved components, such as SO_4^{2-} and Zn^{2+}, had migrated to the NEAR shallow water sites from the tailing.

The FAR shallow water samples (W5–10, 12, 15; pH = 7.9–8.1) had a dissolved Zn concentration in the range of 0.5–0.8 µg/L and W14 (pH = 6.9) had a range of 5.2 µg/L (Fig. 2a; Table A.1), suggesting a solubility equilibrium of zinc hydroxide. Fig. 2b

indicated the variation of Pb concentration in the water samples between the dissolved and total (dissolved plus particulate) values. High Pb concentrations (1–10 µg/L of dissolved and 300–2000 µg/L of total) are usually in the mining area. On the other hand, the Pb concentrations are very low in the dissolved component in the shallow and deep groundwater (0.01–0.04 µg/L), which was lower than 10 µg/L of the WHO water quality guideline (WHO, 2011). The difference in the distribution of dissolved concentration between Zn and Pb (Figs. 2a and 2b) can be explained by the difference in the solubility between the two elements. The pKa values of Zn^{2+}/CO_3^{2-}, $Zn^{2+}/2OH^-$, Zn^{2+}/SO_4^{2-}; Pb^{2+}/CO_3^{2-}, $Pb^{2+}/2OH^-$, Pb^{2+}/SO_4^{2-} and $Pb^{4+}/4OH^-$ are 10.8, 16.9, 2.4; 13.1, 19.9, 7.7 and 64, respectively (Charlot, 2007). As the solubility of lead is smaller than the solubility of zinc at least by two orders of magnitude, a small amount of Pb precipitations had migrated from the mining area in the dissolved form through the aquifer in this area.

On the other hand, the total (dissolved + particulate) Pb concentrations are high (2–100 µg/L) in the shallow groundwater and are relatively high (below 2 µg/L) in some deep groundwater samples (Fig. 2b). As the total concentrations in all samples are higher than the dissolved concentrations by two or three orders of magnitudes, we can consider that the total concentration values are equivalent to the particulate fractions of the water samples. A similar tendency can be recognised with the other heavy metal concentrations of the samples (Table 1; Table A.2). The three FAR shallow wells (W6, 7, 8) exceeded the WHO guideline (10 µg/L) for total-Pb concentration, suggesting a certain amount of suspended matter in the samples.

3.2 A sampling of groundwater filtrates' residue by XRD analysis

The weight of residue on the membrane filter from all samples was too small to measure the residue's weight. Apparently, the amount of residue is the largest in B1, and the order in size is noted in the following: B1> W7> W8 = W6> W3> P1 = P2 (Fig. A.1). The residue's weight from the B1 sample was only several milli-grams. The residue in most of the other samples seems to be very small, like the values of P1 to W3. Thus, few differences are found in the concentration of the major cations between the dissolved and total (dissolved + particulate) components except for the B1 sample having some residue (Table 1; Table A.2).

In the XRD charts of these samples, the filter's strongly reflected peaks and a

significant rise in the background were observed because the PTFE filter papers with the suspended matter were placed on a non-reflective glass plate with glue for XRD measurement. The XRD chart of the unused PTFE filter paper was similar to the reflection pattern of the perfluoroalkoxy (PFA) Teflon (card number 00-070-1340). Therefore, mineral identification of the suspended matter in XRD analysis was performed semi-manually (Table A.3). The XRD peaks of illite and muscovite are similar; thus, it is difficult to determine which mineral is appropriate under these measurement conditions. However, no glittering reflections peculiar to mica were observed with the naked eye on all the filter papers (Fig. A.1), so this study identified the reflection peaks as illite peaks. The XRD analysis shows that the mineral species in the residue of B1 were mainly dolomite ($Ca{\cdot}Mg(CO_3)$) (48%) and illite (49%), and a small percentage of quartz and other clay minerals (montmorillonite, kaolinite). On the contrary, illite (87%) and quartz (10%) were the main mineral species in W7, and the other clay minerals were also detected as minor minerals; this well-water sample was probably skewed due to the addition of a disinfectant several days before the sampling.

Since the residues in W6 and W8 were mainly composed of clay minerals, we can estimate that the suspended matter in the shallow-well water other than W7 is also mainly composed of clay minerals. However, a small amount of dolomite, muscovite and quartz may also be included in the particulate components. Nothing could be identified from the W3 XRD chart like P1 and P2, presumably because of the large increase in the background that the reflection peaks were hidden due to the clay minerals. The major minerals in the soil of this area include clay minerals such as quartz, muscovite and illite; the aquatic layer is composed of dolomite and crystalline schist, so it is probable that these minerals are detected from the groundwater suspensions. Given the samples' pH values and water hardness, it is probable that almost all the dissolved lead had precipitated onto the suspended particles in the shallow aquifer (Brookins, 1988; Marani et al., 1995). Hence, these results explain the difference in Pb concentration between the dissolved and particulate components in Fig. 2b.

[Fig. 3]

Fig. 3 Lead isotopic ratios ($^{206}Pb/^{207}Pb$ vs. $^{208}Pb/^{206}Pb$) in (a) water samples (Total Pb > 5 µg/L); (b) extraction residue component of 1-m core soils (Open circles and squares) and Kabwe galena (PbS) data (Open star; Kamona et al., 1999). Error bars indicate 2 standard errors (SE) of the ratios.

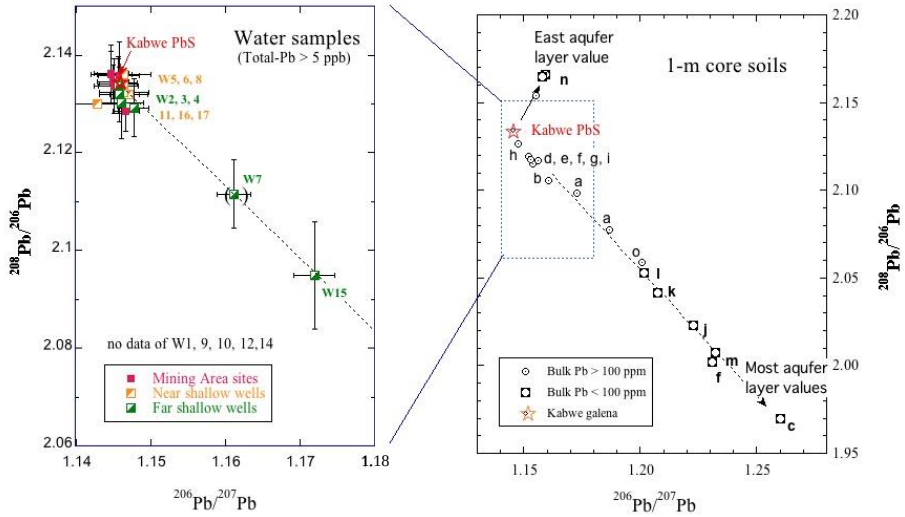

Fig. 3 Lead isotopic ratios ($^{206}Pb/^{207}Pb$ vs. $^{208}Pb/^{206}Pb$) in **(a)** water samples (Total Pb > 5 µg/L); **(b)** extraction residue component of 1-m core soils (Open circles and squares) and Kabwe galena (PbS) data (Open star; Kamona et al., 1999). Error bars indicate 2 standard errors (SE) of the ratios.

3.3 Comparison in Pb isotopic ratios between groundwater and core soil samples

Figs. 3a and 3b show the $^{207}Pb/^{206}Pb$ and $^{208}Pb/^{206}Pb$ ratios in eleven unfiltered shallow groundwater samples (W1–W17), silicate fractions of fifteen core soil samples (a–o in Fig. 1c), and the literature value of Kabwe galena; open star). The soil at the deepest part of the each 1-m cores were analysed to obtain the lead isotopic ratios of the ground soil anterior to the mining activity. However, our analysis showed that some core samples contained Pb bulk contents higher than 100 mg/kg, indicating heavy contamination from the mining. The high Pb content indicates that the Pb isotopic data of soil samples (a–o) should exhibit the mixture of the host rock of each site and Kabwe Ore, even when we tried to remove the pollution from the samples by aqua regia leaching. In Fig. 3b, the Pb isotopic data of all soil samples are aligned with the values for the end-member as noted in the Kabwe galena literature (Baieta et al., 2021; Kamona et al., 1999), except for one site of (n) in the far east area from the tailing. The result suggests that the surface soil samples in this area previously had the Pb isotopic ratios on the line, illustrated as a long-dotted arrow in Fig. 3b, as another end-member of the mixing line.

Fig. 3a indicates that most shallow groundwater samples have the Pb isotopic ratios

similar to the Kabwe galena ratio ($^{206}Pb/^{207}Pb$ = 1.1454 ± 0.0012; $^{208}Pb/^{206}Pb$ = 2.1342 ± 0.0027; Kamona et al., 1999). This result demonstrates that the high Pb concentration (>5 µg/L) of the particulates in most groundwater samples (W2–6, 8, 11, 16 and 17) is significantly derived from the Kabwe Ore. Two samples (W7, W15) were exceptional and displayed isotopic ratios on the mixing line between the Kabwe Ore and the uncontaminated surface soil, assuming that the isotopic ratios are the same as those in the aquifer rocks (3–15 m) in this area. The lowest dissolved Zn and sulphate ions in the W15 sample (Fig. 2a) may allow the exhibition of the Pb isotopic ratios in the 5-m underground aquifer rock at the site. It should be underscored that Kabwe Ore is still the primary end-member of the Pb isotopic ratios in the W15 water sample. However, the W15 well is located 2 km southwest of the tailings deposit, farthest among the shallow wells in this study (Fig. 1). In contrast, some of the lead in W7 water samples can be derived from the anthropogenic chemical input and the water/rock interactions within the aquifer 15 metres in depth. These results suggest that most of the shallow-well water samples (Pb > 5 ppb), including an upstream well 2-km away, were substantially or moderately contaminated by the Kabwe lead Ore, suggesting another alternative migration route of Kabwe lead from the tailing deposit to each well.

The following section describes a preliminary chemical analysis of the soil to consider the migration of lead contamination on the land.

[Fig. 4]

Fig. 4 (a) Pb contents; (b) Pb isotopic ratios ($^{206}Pb/^{207}Pb$ vs. $^{208}Pb/^{206}Pb$); (c) Pb contents vs. $^{208}Pb/^{206}Pb$; (d) $^{206}Pb/^{207}Pb$ vs. 1000/Pb (mg/kg) in bulk and grain-size fractions of surface soils X and Y.

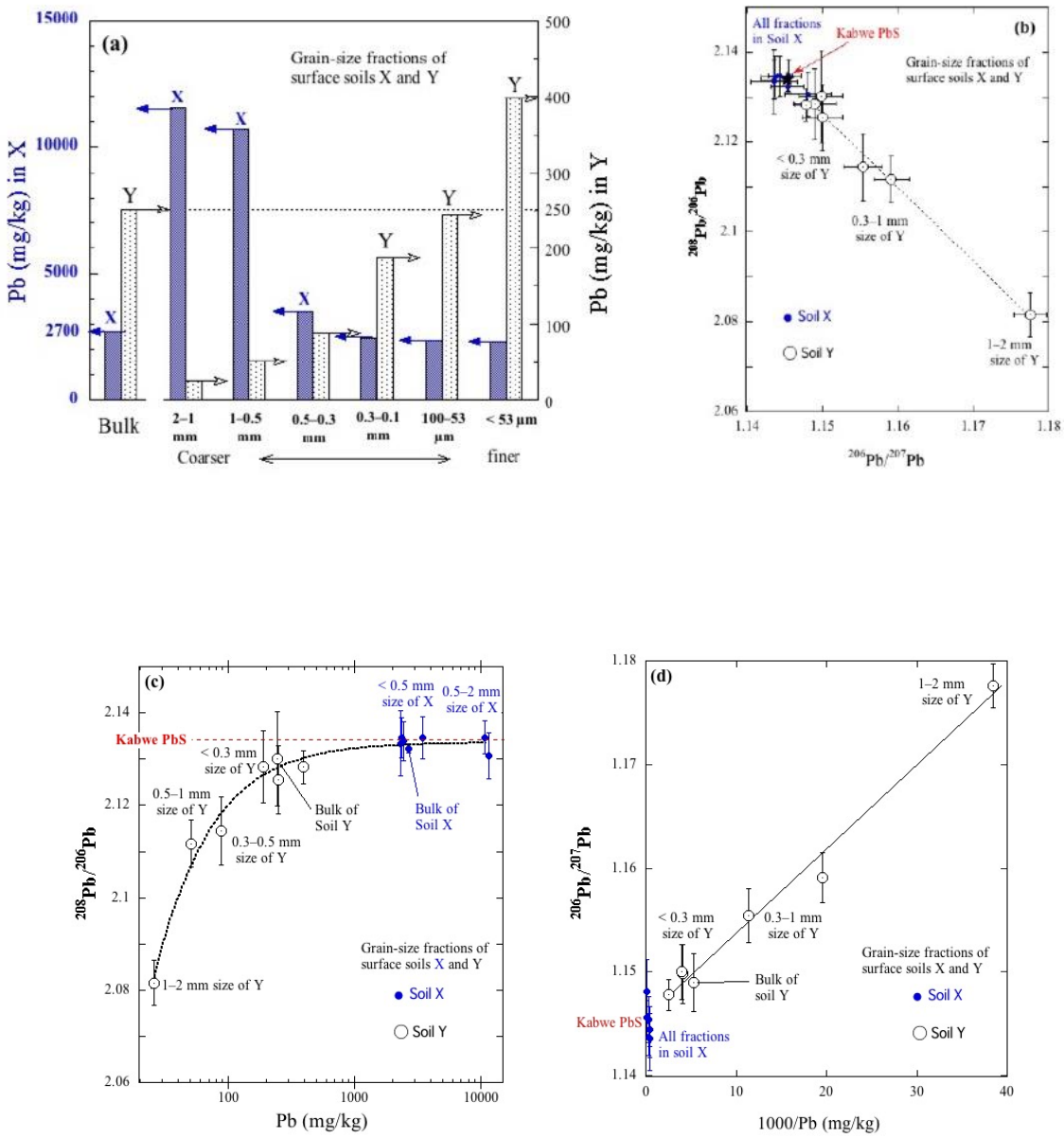

Fig. 4 (a) Pb contents; **(b)** Pb isotopic ratios ($^{206}Pb/^{207}Pb$ vs. $^{208}Pb/^{206}Pb$); **(c)** Pb contents vs. $^{208}Pb/^{206}Pb$; **(d)** $^{206}Pb/^{207}Pb$ vs. 1000/Pb (mg/kg) in bulk and grain-size fractions of surface soils X and Y.

3.4 Chemical composition change in grain-size fractions in two topsoil samples

We chose two topsoil samples for the chemical determination of each of the six categories divided according to the grain size (Fig. 4a; Table A.4): a soil adjacent to the tailings deposit area (X in Fig. 1) and the soil located 2 km northeast of the tailings deposit (Y in Fig. 1). The bulk Pb concentrations in the soils X and Y were 2700 mg/kg and 250 mg/kg, respectively. The Y and W15 sites are near the 200-mg/kg contour line

in the lead concentration distribution map of the surface soil (Kříbek et al., 2019). The Y site faces the W15 site across the direction of the prevailing wind from the tailings deposit. We can assume that the Pb contents in Y mainly consist of two components: 1) airborne lead in the fallout dust from the tailings deposit from Kabwe Pb-Ore; 2) natural Pb inherited from the underlying sediment lithology of the site. In addition, it remains a possibility there are other anthropogenic Pb contributions, e.g. the combustion of leaded gasoline (e.g. Walraven et al., 2014).

The soil X sample (in Fig. 4a) has around 2,500 mg/kg of lead in the fractions, which are finer than 0.3 mm and contain over 1% of lead in a fraction coarser than 0.5 mm of grain size; this is a high concentration for a tailings deposit. These results demonstrate that the coarse grains (>0.5 mm) in soil X are derived from the adjacent tailings deposit, and most of the fine particle fractions (<0.3 mm) probably had come from outside the mining area. Alternatively, the difference in concentration between the two grain-size fractions may be explained at least partly by the leaching of lead during the weathering process of the tailings deposit. The Zn/Pb ratio in bulk soil X, 0.77, is a little lower than the normal range of Zn/Pb ratios (around 1–4) in the tailings deposit (unpublished data; Lee, 2018). However, the higher solubility of zinc rather than lead, as mentioned above, should cause a rapid decrease of the Zn/Pb ratio in the bulk sample during the weathering process (Caroll, 1970). The X soil sample is considered deeply weathered soil because the weight fraction of coarse grains (>0.5 mm) was only a small percentage of the bulk sample. Thus, it is unlikely that the weathering process primarily caused the difference in the lead concentrations among the grain-size fractions of soil X. This data implies that the atmospheric migration of fine soil particles significantly influenced this area's soil chemical composition.

On the tailings deposit, we observed a ground surface where only grains of 2 mm or larger remained on the soil surface (Fig. A.2), indicating that the finer-grained soil particles had already blown away by strong winds and the coarser grains remained. Liu et al. (2019) showed that the threshold wind velocity of 0.3-mm-diameter particles was ca. 6.5 m/s at a water content of 0.1% in a soil modelled by the wind tunnel experiment. The 10^{th} to 90^{th} percentile bands of the average of mean hourly wind speeds are around 3–7 m/s at the dry season, June–September, in Kabwe (Cedar Lake Ventures, 2020). The threshold value of the particle size is 0.3–0.5 mm, which is where the concentration significantly changes in soil X at the vicinity of the tailings deposit.

In soil Y in Fig. 4a, the coarser grain-size fraction is significantly associated with the lower Pb concentrations. The enrichment of heavy metals in the finer size-fraction in the soil was reported in the other areas (Acosta et al., 2009; Liu et al., 2018; Zhang et al., 2013). The coarsest grain fraction of soil Y yielded the lowest concentration,26 mg/kg of Pb. Bowen (1979) calculated 35 mg/kg as the median lead concentration present in ordinary soil samples in the world and estimated 12 mg/kg at prehistoric times. The upper continental crust value, used as a background concentration of sediments, is 40 mg/kg of lead (Taylor and McLennan, 1985). These geochemical data determine the coarsest grain fraction (1–2 mm) of the soil Y to be maintained at the background concentration of lead in the area. Given the prevailing atmospheric migration of finer particles, the change of Pb concentration of the fractions in soil Y can be explained by assuming that the greatest contribution of fallout from the mine dump is found in the finer fractions.

Fig. 4b indicates Pb isotope ratios in bulk and the six grain-size fractions of the two samples X and Y. The isotopic compositions of the soil X (solid circles in Fig. 4b) is rather homogeneous with $^{206}Pb/^{207}Pb$ values of 1.14–1.15 and $^{208}Pb/^{206}Pb$ values of 2.13–2.14, which are consistent with the Kabwe galena ratio ($^{206}Pb/^{207}Pb$ = 1.145 ± 0.001; $^{208}Pb/^{206}Pb$ = 2.134 ± 0.003; closed star in Fig. 4b) by Kamona et al. (1999). The Pb isotope ratio of the coarsest particle fraction (1–2 mm) of soil Y ($^{206}Pb/^{207}Pb$ = 1.178 ± 0.002; $^{208}Pb/^{206}Pb$ = 2.082 ± 0.005; an open circle in Fig. 4b) is on the mixing line between Kabwe galena ratio and the host rock ratios of this area in Fig. 3b. It allows that the ratio represents the natural Pb ratio at the soil Y site. Therefore, the fractions in soil Y have $^{206}Pb/^{207}Pb$ values ranging from 1.15 to 1.18 and $^{208}Pb/^{206}Pb$ varying from 2.08 to 2.14, likely representing a mixture of Kabwe galena Pb from the dumpsite and natural Pb at soil Y site. Monna et al. (2006) reported that the petrol from major companies in these counties has $^{206}Pb/^{207}Pb$ values ranging from 1.057 to 1.096 and $^{208}Pb/^{206}Pb$ varying from 2.330 to 2.366; this plotted region is in the opposite direction of soil Y fractions from Kabwe PbS values. Thus, this data indicates that the contribution of lead gasoline is negligible in this study.

The coarser fractions (0.3–2 mm) of soil Y have the Pb isotopic ratios on the mixing line between the host rock ratios and Kabwe galena ratio in Fig. 2b, thus enabling the identification of the Pb isotopic composition of the natural soil at the site Y. A hyperbolic mixing line can determine the individual isotopic ratios of a mixture of

two different Pb sources (Faure, 2005). Fig. 4c shows the hyperbolic mixing curve defined by $^{208}Pb/^{206}Pb$ and Pb content (mg/kg) in the two end-members ($^{208}Pb/^{206}Pb$ = 2.134, Pb = 1.1%; $^{208}Pb/^{206}Pb$ = 2.0805, Pb = 25 mg/kg), and also the plots in the soil fractions of X and Y, where the error bars are on the mixing curve. The mixing hyperbola can be transformed into a straight line by plotting the isotopic ratio versus Pb content (mg/kg), respectively. Fig. 4d indicates the plot of $^{206}Pb/^{207}Pb$ and respective Pb content in the soil fractions of X and Y, and demonstrates that the data in soil Y is consistent with the straight line (R^2 = 0.983). The data, which is consistent with the models in Figs. 4c and 4d, reveal that the larger content of the fallout dust from the tailings deposit is a finer grain-size fraction in soil Y. For example, the mixing models indicate that 3%–4% of the fraction is finer than 53 μm in soil Y, which had a Pb concentration of 400 mg/kg, was derived from the original mine's deposit.

The change of Pb concentration with grain-size variation in soil Y should be associated with the other soils in the inhabited area. The Pb content contour map in Fig. 1b shows that the high Pb content of the soil (bulk contents > 200 mg/kg) in that area is distributed widely in the inhabited area around the tailing hill. The extrapolation of the change in Fig. 4a indicates that the finer-grain component (<53 μm) in the surrounding soil should have a Pb concentration significantly higher than 400 mg/kg, and usually are re-suspended into the air during the dry season every year. Accordingly in the dry season, the eolian dust in the inhabited areas usually has a particle size component equivalent to the so-called PM2.5 as well as have a Pb concentration significantly higher than 400 mg/kg. [Fig. 5]

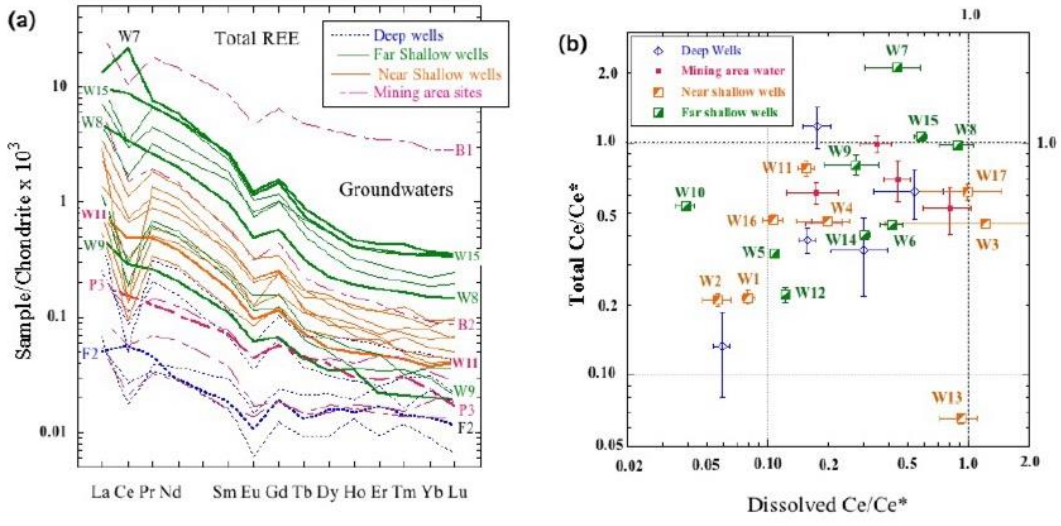

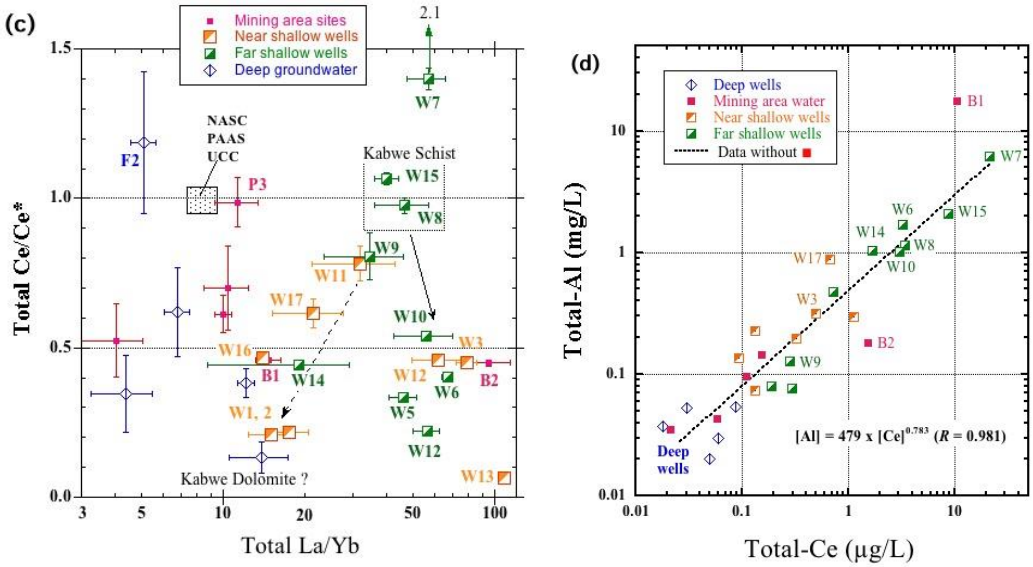

Fig. 5 (a) Rare earth element (REE) patterns; **(b)** Dissolved Ce anomaly vs total Ce anomaly; **(c)** La/Yb ratio vs Ce anomaly; **(d)** Total-Ce concentration (mg/kg) vs total-Al concentration (mg/kg) in water samples. The error bar indicates one standard deviation (SD) of the analysis.

Fig. 5 (a) Rare earth element (REE) patterns; (b) Dissolved Ce anomaly vs total Ce anomaly; (c) La/Yb ratio vs Ce anomaly; (d) Total-Ce concentration (mg/kg) vs total-Al concentration (mg/kg) in water samples. The error bar indicates one standard deviation (SD) of the analysis.

3.5 Rare earth element patterns in the groundwater

Fig. 5a indicates chondrite-normalised (CN) distribution patterns of total (dissolved and particulate) concentrations of the REEs in the groundwater samples. The chondrite values used to normalise the samples (Taylor and McLennan, 1985) are presented in Table A.5. The total REE abundances (∑REE; not including Y) in the deep groundwater, shallow groundwater and mining area water range from 0.10 to 0.57 µg/L, from 0.67 (W1) to 32 µg/L (W7), and from 0.09 to 42 µg/L, respectively. Thus, concentrations of the REEs in these samples range over two orders of magnitude. All patterns have negative slopes from light REE (LREE) to heavy REE (HREE) and negative europium (Eu) anomalies that are common with the upper crustal origin of the majority of silicate rocks through which the groundwater flows (e.g. Johannesson, 2006). A negative Eu

anomaly, where $Eu/Eu^{*} = (Eu)_{CN}/\{(Sm)_{CN}\cdot(Gd)_{CN}\}^{0.5}$, occurs in all groundwater samples (0.5 to 0.8), which is similar to the literature values (ca. 0.65) of North American shale composite (NASC), Post-Archaean average Australian sedimentary rock (PAAS), and average upper continental crust (UCC) (Rollinson, 1993).

In Fig. 5a, one sample (W7: the bold line) has a positive Ce anomaly, and six samples (bold lines) have no or slight Ce anomalies; the other samples have negative Ce anomalies, where $Ce/Ce^{*} = (Ce)_{CN}/\{(La)_{CN}\cdot(Pr)_{CN}\}^{0.5}$. The Ce/Ce^{*} values are ca. 1.02 of NASC, PAAS and UCC. The positive anomaly in sample W7 might be due to the chemical effect dropped into the well for sterilisation. Generally, no or slight Ce anomalies are common with silicate rocks, and negative Ce anomalies are common with marine carbonate rocks, which reflect the prominent negative Ce signature in seawater (Elderfield and Greaves, 1982). For example, (Sholkovitz et al. (1994) reported Ce anomalies which range from 0.12 to 0.47 for seawater from the present Sargasso Sea. Present calcareous deep-sea sediments usually have negative Ce anomalies (Toyoda et al., 1990). Zou et al. (2019) reported a negative Ce anomaly in carbonate rocks after 1.5 Ga, suggesting oxidised Mesoproterozoic shallow seawater. It has been suggested that Kabwe dolomites have been deposited between 880 and 765 Ma (Key et al., 2001). Although the REE patterns of the Kabwe Dolomite remain presently unknown, we typically assume that it has a negative Ce anomaly.

It is well known that the groundwater inherited REE signatures from the host rocks through which they flow (Johannesson et al., 2000). The characteristic of REE patterns of the groundwater samples may be derived from associated aquifer rocks, Kabwe Dolomite and schist of Kangomba Formation. Calcium ion concentrations in W7, W8 and W15 samples without negative Ce anomalies were 28 mg/L, 11 mg/L and 14 mg/L, respectively; whereas, calcium ion concentrations in the other groundwater samples had a range from 39 to 98 mg/L, indicating the contribution of dolomite in the aquifer. On the other hand, Leybourne et al. (2000) and Milodowski et al. (2018) demonstrated that the negative Ce anomaly develops in oxidised groundwaters in the presence of manganese oxides, produced by oxidation Ce^{3+} to Ce^{4+} and preferential removal of Ce^{4+} from the groundwater. Nevertheless, in this study, only three shallow groundwater samples (W3, W13, W14) have soluble Mn concentrations (1187, 18.3, and 5.8 µg/L; Table A.1.), suggesting that reducing conditions also have negative Ce anomalies (Ce/Ce* = 0.45, 0.07 and 0.44; Table A.5). Fig. 5b shows a plot of the Ce anomaly

between the total component (Fig. 5a) and dissolved component (Table A.5: $Ce/Ce^{*} = (Ce)_{CN}/\{(La)_{CN}^{0.66}\cdot(Nd)_{CN}^{0.33}\}$). As all dissolved components also had no or negative Ce anomaly, it is unlikely that only preferential removal of Ce^{4+} from groundwater illustrates the results in Fig. 5b. Therefore, the negative Ce anomalies in the groundwater of this study were mainly induced by the dissolution of negative anomalous dolomite in the aquifer, but the preferential removal of Ce in the oxidative groundwater also contributed significantly. For example, it can be inferred that the positive Ce anomaly in W7 sample is due to the bleaching powder's oxidising action in the well.

Fig. 5c shows a plot between the Ce anomaly and the elemental abundance ratio of La/Yb, a slope from the LREE to the HREE, in the total component of groundwater samples (Fig. 5a). The La/Yb ratio in deep groundwater is 4 to 14, similar to that of the literature values; whereas, the La/Yb ratio in shallow groundwater has an extensive range of 14 to 110. Shallow groundwater samples (W7, 8 and 15) that are not Ce anomalous have a La/Yb ratio of around 50. The three samples (W7, 8 and 15) are likely to be significantly influenced by silicate materials (surface soil or silicate aquifer) due to no negative Ce anomaly and high content of suspended matter in the samples (Table A.5). It is likely that the dolomite component, which has strong negative Ce anomalies and La/Yb ratios of around 10–20. For example, NEAR samples (W1, 2, 11, 16, 17) along one trend (dotted arrow in Fig.5c) were taken from a well in the Kabwe Dolomite area (Fig.1c). However, there is no REE pattern data of these aquifer dolomite rocks in the previous papers and this study. Another trend (straight arrow in Fig.5c) may be an enrichment process of higher soluble elements; LREEs have higher solubilities than HREE (Johannesson, 2006). With variations in the slope of REE pattern of carbonate rocks, the REE contents of ordinary carbonate rocks are lower than that of silicate rocks by one magnitude (Fleet, 1983), so the degree of negative Ce anomalies in total REEs becomes smaller by the existence of suspended silicate particles.

Using three main REEs (La, Ce and Y) that can be expected to have some analytical accuracy, the average proportions of La, Ce and Y in the particulate component were 94%, 97.5% and 87% in total, respectively (Table A.5). This data demonstrates that most REEs have the particulate form (>0.45 μm) in shallow groundwater. Given the pH values of the water samples, it is probable that almost all dissolved REEs had precipitated onto the suspended particles in the shallow aquifer

(Brookins, 1988). Thus, the REE pattern characteristic (Figs. 5a and 5c) is associated with those in the particulate phase. All REEs except Ce in the shallow groundwaters were derived from silicate particulates, while the majority of Ce was derived from silicate components. Fig. 5d indicates a significant positive correlation (R = 0.980) between total-cerium and total-aluminium concentrations in groundwater samples. Aluminium (Al) is the main component of clay minerals, thus enabling the proxy of the particulate silicate component. Furthermore, the Al ion is so insoluble that dissolved Al concentrations were below the determination limits by ICP-OES. Therefore, Fig. 5d proves that most of the Ce in the particulate components was derived from the silicate components in the aquifer schist rock, surface soil and eolian dust around the wells in this area.

Incidentally, the order of total-Al concentrations in groundwater samples in Fig. 5d is B1> W7> W15 = W6> W8 = W10 = W14>W3. It is similar to the order of the apparent amount of residue (B1> W7> W8 = W6> W3; Fig. A.1). Regrettably, some filtration residue samples (W14, W15, W17) had not been retained for further XRD analysis. It was observed that all suspensions of the shallow groundwater samples except W7 had small amounts of clay-like material on the filtrate. The amount of clay minerals produced by weathering crystalline schist in the underground aquifer is smaller than that produced on land (Caroll, 1970). Since the lead concentration in the schist is at a natural level, assuming that the contribution of the schist from the aquifer was great, the high lead content in the suspended matter cannot be explained. However, with no contribution from the aquifer to the formation of suspended matter in groundwater the negative Ce anomalies in the suspensions cannot be explained.

Fig. 5b indicates that the dissolved components of well water away from the dolomite layer (W10, 14, 15) also have negative Ce anomalies (Ce/Ce^{*} = 0.04, 0.3, 0.6, respectively). It may demonstrate that the dissolved dolomite-derived REEs migrated as colloidal hydroxide particles (<0.45 μm diameter) through the aquifer to the well sites and was adsorbed by the suspended particles in the groundwater. In the following section, we will assume that most of the silicate components in the suspension are derived from the surface soil and air dust.

[Fig. 6]

Fig. 6 (a) Total-Ce concentration vs. total-Pb concentration; (b) Total-Al concentration

vs. total-Pb concentrations in the water samples.

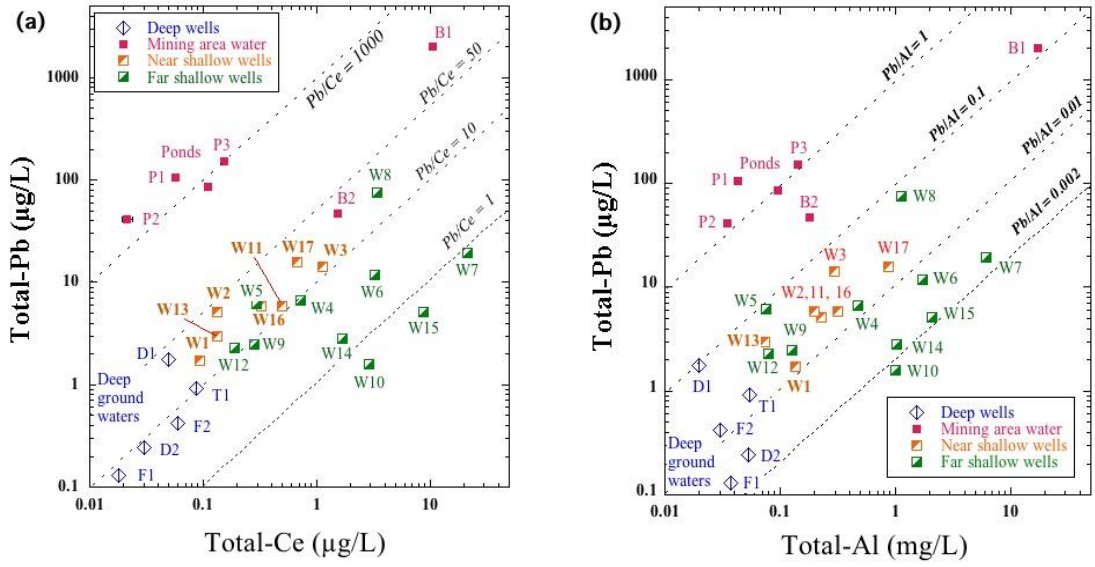

Fig. 6 (a) Total-Ce concentration vs. total-Pb concentration; **(b)** Total-Al concentration vs. total-Pb concentrations in the water samples.

3.6 Estimation of Pb levels in the suspended matter in groundwater and eolian dust

Figs. 5d, 6a and 6b show that the five deep groundwater samples have low total-Ce (<0.1µg/L) and low total-Al (<0.06 µg/L), suggesting that aquifer-derived silicates have a low concentration in the deep groundwater in this area. At the water factories (F1, F2), deep groundwater is pumped, passing through a sedimentation tank pool, and is supplied as tap water (e.g. T1) immediately after adding the disinfectant solution. After pumping at the F1 site, we immediately collected the deep groundwater; this explains why the F1 site has the lowest total-Pb concentration (0.11 µg/L) even though it is in the mining area. At D sites, deep groundwater was pumped up to the water tank to a high position in the water tower and stored. At the D1 site, the groundwater may have been exposed to air during its storage, resulting in a high total-Pb concentration of (1.75 µg/L).

In Fig. 6a, the pond waters in the mining area have ratios of Pb/Ce = ca.1000. The Pb/Ce ratio of the deep groundwater samples and most of the shallow groundwater samples are in the range of 10–40. It may be explained that the suspended matter has a

Pb/Ce ratio in the range of 10 to 40 in areas outside the tailings deposit. The other shallow groundwater samples (W7, 10, 14, 15) have ratios of Pb/Ce = ca. 1. Three samples (W10, 14, 15) are located the farthest, west and southwest, from the tailings deposit among the shallow wells. The Pb/Ce ratio of the suspended matter may decrease with the distance from the tailings deposit, like the distribution of Pb contents in the topsoil (Fig. 1b; Kříbek et al., 2019).

The distribution and trends of data in Pb vs Ce contents (Fig. 6a) are similar to those in Pb vs Al contents (Fig. 6b), indicating that both tables demonstrate approximate Pb amounts in the silicate particulates of each water sample. The Al and Ce contents in each sample (Figs. 6a and 6b) also match the photo of the residue on the filter paper (Fig. A.1). The pond waters in the mining area have ratios of Pb/Al = ca. 1. The Pb/Al ratio of most shallow groundwater samples is in the range of 0.01–0.1, indicating that the aeolian dust may have a Pb/Al ratio in the range of 0.01–0.1 in immediate areas from the tailing. It is indicated that dust particles with Pb/Al = ca. 1 in the mining area have been diluted by the other dust derived from uncontaminated soil during the migration from the tailing deposit to the surrounding area. The other shallow groundwater samples (W7, 10, 14, 15) have Pb/Al ratios of Pb/Al = ca. 0.002. It may indicate that the Pb/Al ratio in the aeolian dust decreases to ca. 0.002 at W7, 10, 14, 15, as mentioned above by the Pb/Ce ratio.

The suspended matter in the pond waters in the mining area have substantial quantities of lead as noted in Figs. 6a and 6b: Pb(μg/L)/Ce(μg/L) = 1000 and Pb(μg/L)/Al(mg/L) = 1. If particulates in the pond waters (P1, P2 and P3) had a chemical matrix with an ordinary sedimentary composition, the particulate Pb content would be around 7%. The Ce contents in NASC, PAAS and UCC are 67.0, 79.6 and 64 mg/kg, respectively, and the Al contents in most general reference materials of silicate sediment is 6% to 8% (e.g., JLk-1, STSD-4, GSD-1; Potts et al., 1992). However, slag deposits are very different from normal sediments; they have a much lower Al and Ce content (less than 7%) than typical sediments. In Fig. 4, the coarse grain (0.5–2 mm) fraction at site X has 1.1%, suggesting the coarse grain was derived from the slag deposits. Ettler et al. (2020) analysed four representative samples from southeast and west slag deposits in the tailing area (dotted hatch pattern area in Fig. 1c) and reported that bulk slag, slag dust fraction (<48 μm), and slag dust fraction (<10 μm) averaged 1%, 4% and 4.8% of Pb, respectively. The southeast slag deposit is near site X in this

study (Fig. 1c). The estimation that the suspended matter has at most several percent of lead in the pond waters (P1, P2 and P3) in the mining area (Fig. 6b) is also consistent with the data by Ettler et al. (2020).

In most shallow groundwaters (Figs. 6a and 6b), the suspended matter has Pb/Ce = 10–40 and Pb/Al = 0.01–0.1, indicating estimated Pb contents are 700–2800 mg/L and 700–7000 mg/L, on the above assumption. In W7, W10, W14 and W15 well sites (Fig. 6b), the suspended matter has Pb/Al = ca. 0.02, indicating the Pb contents are 140 mg/L, respectively, regarding the above assumption. The W15 well site is located the farthest from the dolomite zone (Fig. 1c). In Fig. 3, W7 and W15 have exceptional isotopic ratios on the mixing line between the Kabwe Ore and the uncontaminated host rock in this area. Although no isotopic Pb ratios in W10 and W14 were measured due to the low Pb concentration (Total-Pb < 5 μg/L) in this study, we could expect that these ratios would also be on the mixing line in Fig. 3. [Fig. 7]

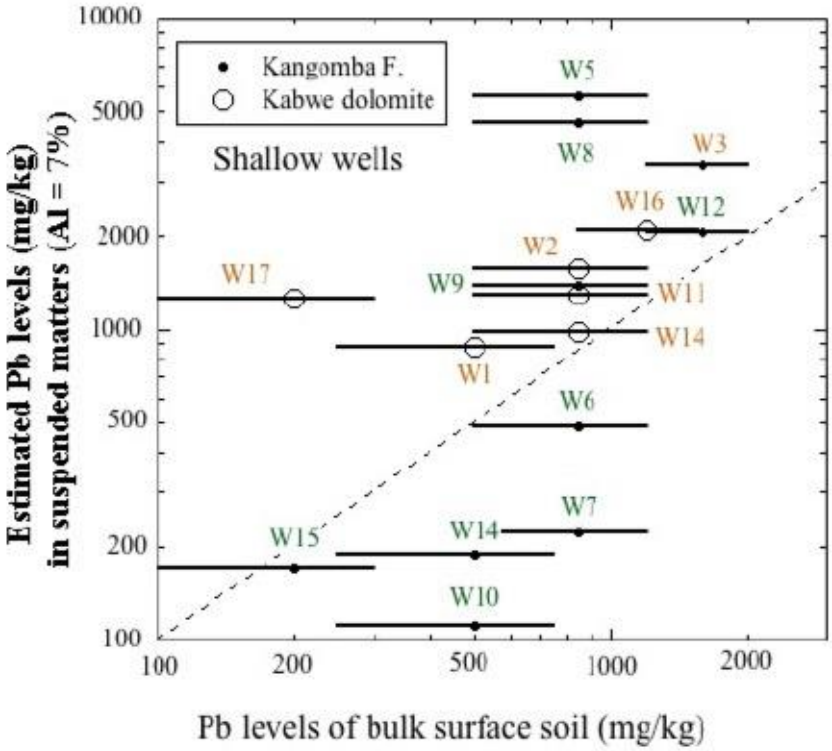

Fig. 7 The comparison between probable Pb concentration in bulk surface soils at each shallow well by the contour map (Kříbek et al., 2019) and estimated Pb concentrations (mg/kg) in a suspended matter in each well-water sample on the assumption that the Al concentration in the suspended solids is 7%.

Fig. 7 The comparison between probable Pb concentration in bulk surface soils at each shallow well by the contour map (Kříbek et al., 2019) and estimated Pb concentrations (mg/kg) in a suspended matter in each well-water sample on the assumption that the Al concentration in the suspended solids is 7%.

Fig. 7 demonstrates the relationship between estimated Pb concentrations in a suspended matter in shallow-well water and probable Pb concentrations of bulk surface soil at the well sites. The Pb soil concentration ranges of each site were tried to trace from the contour maps of Pb concentration (Kříbek et al., 2019; unpublished data: Lee, 2018); 200 ± 100 mg/kg, 500 ± 200 mg/kg, 850 ± 300 mg/kg, 1200 ± 350 mg/kg, 1600 ± 400 mg/kg. If the suspended matter in the well water is derived from the inflow of soil around the well by some route, Fig. 7 should give a strong positive correlation. The weak correlation (R = 0.19) suggests an alternative hypothesis that the suspension particles are mainly derived from atmospheric fallout. No significant relationship with the permeable layer pollution (Near or Far) and the surface geology (Kamgomba Formation or Kabwe Dolomite) is found in the data in Fig. 7, which also supports the hypothesis. This hypothesis explains that the Pb concentration in the suspended matter in the well water of W5 and W8 in the zone where the soil lead concentration is 500 to 1200 mg/kg was estimated to be about 0.5%. We have already described that the finer grain-size fraction is markedly associated with the higher Pb concentration (Fig. 4). On the other hand, the Pb concentration in the suspended matter in the well water of W10 and W14 in the zone where the soil lead concentration is around 500 mg/kg is estimated to be 100–200 mg/kg.

Assuming that the source of the suspended matter in the well-water samples is the atmospheric dust fallout, we calculated how many days it floated at the well water's surface as follows. The Stokes' law equation indicates that the time required for a sphere with a density of 2.5 to settle down 10 cm in the water are 8.6 hours and 5.7 days for the diameters of 2 μm, and 0.5 μm, respectively, at 20 °C (e.g. Rząsa and Owczarzak, 2013). Because most of the suspension was filtered through a 0.45 μm filter, its particle size should be greater than 0.45 μm. The inhabitants are usually collecting well water from a half of metre below the water's surface. Therefore, it is conceivable that dust particles with a particle size of 0.45 μm to a few μm typically exist as suspensions in the well water. This consideration may explain the discrepancy in Fig. 7 that the Pb/Al

ratio in the well-water samples is a proxy for fallout in the past few weeks, while the surface soil contour map results from the cumulative value of fallout. When utilising Stokes's law, the calculation also suggests that suspended matter in well water in the dry season (November to March) could not be derived from the migration of surface soil into the shallow groundwater aquifer following the heavy seasonal rains (May to September). Similarly, the suspended matter (>0.5 μm size) moved from the aquifer schist to the bottom of the water column of the well.

Given that the suspended solids in groundwater are finer fractions like dust than the surrounding soil, the assumption that the Al concentration in the suspended solids is 7% also needs to be reviewed. The XRD results estimated that the main component in the suspended matter is a clay mineral such as illite. The Al contents of montmorillonite, illite and kaolinite are typically 7%–11%, ca. 16% and ca. 21%, respectively (Miyawaki et al., 2010). Therefore, the estimated Pb contents in the dust in Fig. 7, calculated from the measured Pb/Al ratio, were the lower limit values. For example, our result is that the Pb levels in a suspended matter in W5 and W8 wells were estimated to be at least ca. 0.5%.

4. Conclusions

Our results suggest that the so-called PM2.5 material in the atmosphere in some residential areas sometimes may have a concentration of thousands (mg/kg) of lead. As the airborne contaminant of this grain size accumulates in the alveoli of the human lung, it could lead to mortality (Dockery et al., 1993). This finding highlights an urgent issue on the health hazard of the local people. In the residential areas, even clean water, such as deep groundwater, may contain more lead than permitted by the WHO guidelines if exposed to the air for long periods of time. This paper assumed that the shallow well is a natural trap of airborne fine-grain PMs. However, further research is needed to determine whether the method utilising a rough estimation of the Pb concentration of dust at the well sites is correct.

Acknowledgements

This research was supported by JST/JICA, SATREPS (Science and Technology Research Partnership for Sustainable Development; No. JPMJSA1501) and aXis (Accelerating Social Implementation for SDGs Achievement; No. JPMJAS2001)

funded by JST. We are grateful to Kazuya Nagaishi, Marine Works Japan Ltd. for assistance in analyses using MC-ICP-MS installed in the Kochi Core Center and to Prof. Kei Okamura for arranging the Center for Advanced Marine Core Research, Kochi University (CMCR) Nationwide Joint Use System (17A025). The authors are thankful to technical staff members at Open Facility, Hokkaido University, for facilitating ICP-QQQ and XRD systems. The ICP-OES and ion analyzer setting at FEES had been supported by Grant-in-Aid for Scientific Research (08409001, 17340148) of MEXT, Japan. The authors would like to thank Enago (www.enago.jp) for the English language review. One half of this study's data is from S. Nakano's Master thesis (2017).

References

Acosta, J.A., Cano, A.F., Arocena, J.M., Debela, F., Martínez-Martínez, S., 2009. Distribution of metals in soil particle size fractions and its implication to risk assessment of playgrounds in Murcia City (Spain). Geoderma 149, 101–109. https://doi.org/10.1016/j.geoderma.2008.11.034

Ando, A., Kamioka, H., Terashima, S., Itoh, S., 1989. 1988 values for GSJ rock reference samples, 'Igneous rock series'. Geochem. J. 23, 143–148. https://doi.org/10.2343/geochemj.23.143

Aničić, M., Mijić, Z., Kuzmanoski, M., Stojić, A., Tomašević, M., Rajšić, S., Tasić, M., 2012. A study of airborne trace elements in belgrade urabn area: Instumental and active biomonitoring approch, in: Diego A. De Leon; Paloma Raquel Aragon (Ed.), Trace Elements. Nova Science Publishers, Inc., pp. 1–30.

Baieta, R., Mihaljevič, M., Ettler, V., Vaněk, A., Penížek, V., Trubač, J., Kříbek, B., Ježek, J., Svoboda, M., Sracek, O., Nyambe, I., 2021. Depicting the historical pollution in a Pb–Zn mining/smelting site in Kabwe (Zambia) using tree rings. J. African Earth Sci. 181, 104246. https://doi.org/10.1016/j.jafrearsci.2021.104246

Blacksmith Institute, 2013. The Worlds Worst 2013: the Top Ten Toxic Threats Cleanup, Progress, and Ongoing Challenges Table 19.

Bose-O'Reilly, S., Yabe, J., Makumba, J., Schutzmeier, P., Ericson, B., Caravanos, J., 2018. Lead intoxicated children in Kabwe, Zambia. Environ. Res. 165, 420–424. https://doi.org/10.1016/j.envres.2017.10.024

Bowen, H.J.M., 1979. Environmental chemistry of the elements. Academic Press, London.

Brookins, D.G., 1988. Eh-ph diagrams for geochemistry. Springer-Verlag, Tokyo.

Caroll, D., 1970. Rock Weathering, Plenum Press. Plenum Press, New York.

Cedar Lake Ventures, I., 2020. Average Weather in Kabwe Zambia; Spark, Weather. URL https://weatherspark.com/y/95291/Average-Weather-in-Kabwe-Zambia-Year-Round

Charlot, G., 2007. Qualitative Inorganic Analysis. Thomas Pr. 368 p. ISBN: 978-1406747898

CMS, 2005. SAFETY DATA SHEET. IMt-2. CLAY Miner. Soc. URLhttps://www.google.co.jp/url?sa=t&rct=j&q=&esrc=s&source=web&cd=&ved=2ahUKEwi0t96Im_3xAhVuQfUHHVofA7wQFjAAegQIBRAD&url=https%3A%2F%2Fwww.agry.purdue.edu%2Fcjohnston%2Fsourceclays%2FPDF%2FIMt-2.pdf&usg=AOvVaw2R8zjVgPm6c1F8F4aemVb6

Corapcioglu, M.Y., Jiang, S., 1993. Colloid- facilitated groundwater contaminant transport. Water Resour. Res. 29, 2215–2226. https://doi.org/10.1029/93WR00404

Csavina, J., Field, J., Taylor, M.P., Gao, S., Landázuri, A., Betterton, E.A., Sáez, A.E., 2012. A review on the importance of metals and metalloids in atmospheric dust and aerosol from mining operations. Sci. Total Environ. 433, 58–73. https://doi.org/10.1016/j.scitotenv.2012.06.013

Deniel, C., Pin, C., 2001. Single-stage method for the simultaneous isolation of lead and strontium from silicate samples for isotopic measurements. Anal. Chim. Acta 426, 95–103. https://doi.org/10.1016/S0003-2670(00)01185-5

Dockery, D., Pope, C., Xu, X. et al., 1993. An Association between Air Pollution and Mortality in Six U.S. Cities. N. Engl. J. Med. 329, 977–986. https://doi.org/10.1056/NEJM199309303291401

Elderfield, H., Greaves, M.J., 1982. The rare earth elements in seawater. Nature 296, 214–219. https://doi.org/10.1038/296214a0

Ettler, V., 2015. Soil contamination near non-ferrous metal smelters: A review. Appl. Geochemistry 64, 56–74. https://doi.org/10.1016/j.apgeochem.2015.09.020

Ettler, V., Štěpánek, D., Mihaljevič, M., Drahota, P., Jedlicka, R., Kříbek, B., Vaněk, A., Penížek, V., Sracek, O., Nyambe, I., 2020. Slag dusts from Kabwe (Zambia): Contaminant mineralogy and oral bioaccessibility. Chemosphere 260. https://doi.org/10.1016/j.chemosphere.2020.127642

Faure, G. and Mensing, T.M., 2005. Isotopes: principles and applications, 3rd ed. ed.

Wiley, Hoboken, N.J.
Geochemistry group, GSJ (Geological Survey of Japan) Geochemical Reference Samples Database. URL https://gbank.gsj.jp/geostandards/welcome.html
Ghorbel, M., Munoz, M., Solmon, F., 2014. Health hazard prospecting by modeling wind transfer of metal-bearing dust from mining waste dumps: application to Jebel Ressas Pb–Zn–Cd abandoned mining site (Tunisia). Environ. Geochem. Health 36, 935–951. https://doi.org/10.1007/s10653-014-9610-y
Hillier, S., 2000. Accurate quantitative analysis of clay and other minerals in sandstones by XRD: comparison of a Rietveld and a reference intensity ratio (RIR) method and the importance of sample preparation. Clay Miner. 35, 291–302. https://doi.org/10.1180/000985500546666
Houston, J.F.T., 1982. Rainfall and recharge to a dolomite aquifer in a semi-arid climate at Kabwe, Zambia. J. Hydrol. 59, 173–187. https://doi.org/10.1016/0022-1694(82)90010-5
Johannesson, K.H., 2006. Rare Earth Elements in Groundwater Flow Systems. Springer, Dordrecht.
Johannesson, K.H., Zhou, X., Guo, C., Stetzenbach, K.J., Hodge, V.F., 2000. Origin of rare earth element signatures in groundwaters of circumneutral pH from southern Nevada and eastern California, USA. Chem. Geol. 164, 239–257. https://doi.org/10.1016/S0009-2541(99)00152-7
Kamona, A.F., Friedrich, G.H., 2007. Geology, mineralogy and stable isotope geochemistry of the Kabwe carbonate-hosted Pb-Zn deposit, Central Zambia. Ore Geol. Rev. 30, 217–243. https://doi.org/10.1016/j.oregeorev.2006.02.003
Kamona, A.F., Lévêque, J., Friedrich, G., Haack, U., 1999. Lead isotopes of the carbonate-hosted Kabwe, Tsumeb, and Kipushi Pb-Zn-Cu sulphide deposits in relation to Pan African orogenesis in the Damaran-Lufilian Fold Belt of Central Africa. Miner. Depos. 34, 273–283. https://doi.org/10.1007/s001260050203
Kataba, A., Nakayama, S.M.M., Nakata, H., Toyomaki, H., Yohannes, Y.B., Yabe, J., Muzandu, K., Zyambo, G., Kubota, A., Matsukawa, T., Yokoyama, K., Ikenaka, Y., Ishizuka, M., 2021. An investigation of the wild rat crown incisor as an indicator of lead (Pb) exposure using inductively couple plasma mass spectrometry (ICP-MS) and laser ablation ICP-MS. Int. J. Environ. Res. Public Health 18, 1–15. https://doi.org/10.3390/ijerph18020767

Key, R.M., Liyungu, A.K., Njamu, F.M., Somwe, V., Banda, J., Mosley, P.N., Armstrong, R.A., 2001. The western arm of the Lufilian Arc in NW Zambia and its potential for copper mineralization. J. African Earth Sci. 33, 503–528. https://doi.org/10.1016/s0899-5362(01)00098-7

Kossoff, D., Dubbin, W.E., Alfredsson, M., Edwards, S.J., Macklin, M.G., Hudson-Edwards, K.A., 2014. Mine tailings dams: Characteristics, failure, environmental impacts, and remediation. Appl. Geochemistry 51, 229–245. https://doi.org/10.1016/j.apgeochem.2014.09.010

Kříbek, B., Nyambe, I., Majer, V., Knésl, I., Mihaljevič, M., Ettler, V., Vaněk, A., Penížek, V., Sracek, O., 2019. Soil contamination near the Kabwe Pb-Zn smelter in Zambia: Environmental impacts and remediation measures proposal. J. Geochemical Explor. 197, 159–173. https://doi.org/10.1016/j.gexplo.2018.11.018

Lee, C.W., 2018. Spatial distribution of heavy metals around the abandoned mine in Kabwe, Zambia. Master thesis, Graduate school of Environmental Science, Hokkaido University.

Leybourne, M.I., Goodfellow, W.D., Boyle, D.R., Hall, G.M., 2000. Rapid development of negative Ce anomalies in surface waters and contrasting REE patterns in groundwaters associated with Zn-Pb massive sulphide deposits. Appl. Geochemistry 15, 695–723. https://doi.org/10.1016/S0883-2927(99)00096-7

Liu, B., Qu, J., Ning, D., Han, Q., Yin, D., Du, P., 2019. WECON: A model to estimate wind erosion from disturbed surfaces. Catena 172, 266–273. https://doi.org/10.1016/j.catena.2018.08.037

Liu, G., Wang, Juan, Liu, Xuan, Liu, Xinhui, Li, X., Ren, Y., Wang, Jing, Dong, L., 2018. Partitioning and geochemical fractions of heavy metals from geogenic and anthropogenic sources in various soil particle size fractions. Geoderma 312, 104–113. https://doi.org/10.1016/j.geoderma.2017.10.013

Marani, D., Macchi, G., Pagano, M., 1995. Lead precipitation in the presence of sulphate and carbonate: Testing of thermodynamic predictions. Water Res. 29, 1085–1092. https://doi.org/10.1016/0043-1354(94)00232-V

Milodowski, A.E., Bath, A., Norris, S., 2018. Palaeohydrogeology using geochemical, isotopic and mineralogical analyses: Salinity and redox evolution in a deep groundwater system through Quaternary glacial cycles. Appl. Geochemistry 97, 40–60. https://doi.org/10.1016/j.apgeochem.2018.07.008

Miyawaki, R., Sano, T., Ohashi, F., Suzuki, M., Kogure, T., Okumura, T., Kameda, J., Umezone, T., Sato, T., Chino, D., Hiroyama, K., Yamada, H., Tamura, K., Morimoto, K., Uehara, S., Hatta, T., 2010. Some Reference Data for the JCSS Clay Specimens. J. Clay Sci. Soc. Japan (in Japanese) 48, 158–198. https://doi.org/10.11362/jcssjnendokagaku.48.4_158

Monna, F., Poujol, M., Losno, R., Dominik, J., Annegarn, H., Coetzee, H., 2006. Origin of atmospheric lead in Johannesburg, South Africa. Atmos. Environ. 40, 6554–6566. https://doi.org/10.1016/j.atmosenv.2006.05.064

Nakano, S. 2017. Lead and lead isotope ratio analysis in water samples around the Kabwe mine, Zambia. Master thesis, Graduate school of Environmental Science, Hokkaido University.

Nakata, H., Nakayama, S.M.M., Kataba, A., Yohannes, Y.B., Ikenaka, Y., Ishizuka, M., 2021a. Evaluation of the ameliorative effect of Spirulina (Arthrospira platensis) supplementation on parameters relating to lead poisoning and obesity in C57BL/6J mice. J. Funct. Foods 77, 104344. https://doi.org/10.1016/j.jff.2020.104344

Nakata, H., Tohyama, H., Fujita, W., Nakayama, S.M.M., Ishizuka, M., Yabe, J., Munyinda, N.S., Sakala, D., Choongo, K., Yamasaki, S., Nagai, N., Yoshida, T., Saito, T., 2021b. The impact of elevated blood lead levels in children on maternal health-related quality of life. Chemosphere 279, 130490. https://doi.org/10.1016/j.chemosphere.2021.130490

Nakayama, S.M.M., Ikenaka, Y., Hamada, K., Muzandu, K., Choongo, K., Teraoka, H., Mizuno, N., Ishizuka, M., 2011. Metal and metalloid contamination in roadside soil and wild rats around a Pb-Zn mine in Kabwe, Zambia. Environ. Pollut. 159, 175–181. https://doi.org/10.1016/j.envpol.2010.09.007

Nakayama, S.M.M., Ikenaka, Y., Hamada, K., Muzandu, K., Choongo, K., Yabe, J., Umemura, T., Ishizuka, M., 2013. Accumulation and biological effects of metals in wild rats in mining areas of Zambia. Environ. Monit. Assess. 185, 4907–4918. https://doi.org/10.1007/s10661-012-2912-6

Nakayama, S.M.M., Nakata, H., Ikenaka, Y., Yabe, J., Oroszlany, B., Yohannes, Y.B., Bortey-Sam, N., Muzandu, K., Choongo, K., Kuritani, T., Nakagawa, M., Ishizuka, M., 2019. One year exposure to Cd- and Pb-contaminated soil causes metal accumulation and alteration of global DNA methylation in rats. Environ. Pollut. 252, 1267–1276. https://doi.org/10.1016/j.envpol.2019.05.038

Phiri, A., 2016. Risks of Domestic Underground Water Sources in Informal Settlement in Kabwe – Zambia. Environ. Pollut. 5, 1. https://doi.org/10.5539/ep.v5n2p1

Potts, P. J.; Tindle, A. G. ; Webb, P.C., 1992. Geochemical Reference Material Compositions: Rocks, Minerals, Sediments, Soils, Carbonates, Refractories & Ores Used in Research & Industry. CRC Press, Boca Raton.

Rollinson, H.R., 1993. Using geochemical data : evaluation, presentation, interpretation. Routledge, London.

Rząsa, S., Owczarzak, W., 2013. Methods for the granulometric analysis of soil for science and practice. Polish J. Soil Sci. 46, 1–50.

Sholkovitz, E.R., Landing, W.M., Lewis, B.L., 1994. Ocean particle chemistry: The fractionation of rare earth elements between suspended particles and seawater. Geochim. Cosmochim. Acta 58, 1567–1579. https://doi.org/10.1016/0016-7037(94)90559-2

Sorensen, J.P.R., Lapworth, D.J., Nkhuwa, D.C.W., Stuart, M.E., Gooddy, D.C., Bell, R.A., Chirwa, M., Kabika, J., Liemisa, M., Chibesa, M., Pedley, S., 2015. Emerging contaminants in urban groundwater sources in Africa. Water Res. 72, 51–63. https://doi.org/10.1016/j.watres.2014.08.002

Southwood, M., Cairncross, B., Rumsey, M.S., 2019. Minerals of the Kabwe ("Broken Hill") Mine, Central Province, Zambia. Rocks Miner. 94, 114–149. https://doi.org/10.1080/00357529.2019.1530038

Tanimizu, M., Ishikawa, T., 2006. Development of rapid and precise Pb isotope analytical techniques using MC-ICP-MS and new results for GSJ rock reference samples. Geochem. J. 40, 121–133. https://doi.org/10.2343/geochemj.40.121

Taylor, S. R., and McLennan, S.M., 1985. The Continental Crust: Its Composition and Evolution: An Examination of the Geochemical Record Preserved in Sedimentary Rocks. Blackwell Scientific Publications, Oxford.

Tembo, B.D., Sichilongo, K., Cernak, J., 2006. Distribution of copper, lead, cadmium and zinc concentrations in soils around Kabwe town in Zambia. Chemosphere 63, 497–501. https://doi.org/10.1016/j.chemosphere.2005.08.002

Toyoda, K.; Haraguchi, H., 1987. Geochemical Characterization of Geological Standard Rock Samples from Rare Earth Elements Distribution Pattern Measured by Inductively Coupled Plasma Atomic Emission Spectrometry. Bull. Chem. Soc. Jpn. 60, 933–939.

Toyoda, K., Nakamura, Y., Masuda, A., 1990. Rare earth elements of Pacific pelagic sediments. Geochim. Cosmochim. Acta 54, 1093–1103.

Uddh Söderberg, T., Berggren Kleja, D., Åström, M., Jarsjö, J., Fröberg, M., Svensson, A., Augustsson, A., 2019. Metal solubility and transport at a contaminated landfill site – From the source zone into the groundwater. Sci. Total Environ. 668, 1064–1076. https://doi.org/10.1016/j.scitotenv.2019.03.013

Walraven, N., van Os, B.J.H., Klaver, G.T., Middelburg, J.J., Davies, G.R., 2014. The lead (Pb) isotope signature, behaviour and fate of traffic-related lead pollution in roadside soils in The Netherlands. Sci. Total Environ. 472, 888–900. https://doi.org/10.1016/j.scitotenv.2013.11.110

WHO, 2011. Guidelines for Drinking-water Quality. Geneve.

Wolfe, P.J., Giang, A., Ashok, A., Selin, N.E., Barrett, S.R.H., 2016. Costs of IQ loss from leaded aviation gasoline emissions. Environ. Sci. Technol. 50, 9026–9033. https://doi.org/10.1021/acs.est.6b02910

Yabe, J., Nakayama, S.M.M., Ikenaka, Y., Yohannes, Y.B., Bortey-Sam, N., Kabalo, A.N., Ntapisha, J., Mizukawa, H., Umemura, T., Ishizuka, M., 2018. Lead and cadmium excretion in feces and urine of children from polluted townships near a lead-zinc mine in Kabwe, Zambia. Chemosphere 202, 48–55. https://doi.org/10.1016/j.chemosphere.2018.03.079

Yabe, J., Nakayama, S.M.M., Ikenaka, Y., Yohannes, Y.B., Bortey-Sam, N., Oroszlany, B., Muzandu, K., Choongo, K., Kabalo, A.N., Ntapisha, J., Mweene, A., Umemura, T., Ishizuka, M., 2015. Lead poisoning in children from townships in the vicinity of a lead-zinc mine in Kabwe, Zambia. Chemosphere 119, 941–947. https://doi.org/10.1016/j.chemosphere.2014.09.028

Yohannes, Y.B., Nakayama, S.M., Yabe, J., Nakata, H., Toyomaki, H., Kataba, A., Muzandu, K., Ikenaka, Y., Choongo, K., Ishizuka, M., 2020. Blood lead levels and aberrant DNA methylation of the ALAD and p16 gene promoters in children exposed to environmental-lead. Environ. Res. 188, 109759. https://doi.org/10.1016/j.envres.2020.109759

Yohannes, Y.B., Nakayama, S.M.M., Yabe, J., Toyomaki, H., Kataba, A., Nakata, H., Muzandu, K., Ikenaka, Y., Choongo, K., Ishizuka, M., 2021. Delta-aminolevulinic acid dehydratase (ALAD) and vitamin D receptor (VDR) genes polymorphisms in children residing in an abandoned lead‐zinc mine area in Kabwe, Zambia. Meta

Gene 27, 100838. https://doi.org/10.1016/j.mgene.2020.100838

ZCCM-IH, 2004. December 2004, Kabwe scoping and design study phase 1 completion report. Kitwe, Zambia. https://doi.org/10.1007/s00418-004-0740-7

Zhang, H., Luo, Y., Makino, T., Wu, L., Nanzyo, M., 2013. The heavy metal partition in size-fractions of the fine particles in agricultural soils contaminated by waste water and smelter dust. J. Hazard. Mater. 248–249, 303–312. https://doi.org/10.1016/j.jhazmat.2013.01.019

Zou, Y., Liu, D., Zhao, F., Kuang, H., Sun, Y., Cheng, J., 2019. Chemostratigraphy of the Mesoproterozoic Shennongjia Group, Yangtze Craton (South China): Implications for oxidized shallow seawaters. J. Asian Earth Sci. 179, 399–415. https://doi.org/10.1016/j.jseaes.2019.02.026

Appendix Captions

Fig. A.1. Picture of the groundwater samples" residue on the filter.

Fig. A.2. Pictures of the site's ground surface on the tailing hill. The footprints in the picture illustrate the scale of the picture.

Table A.1. Dissolved (<0.45 μm) minor element concentration and the total-Pb isotopic ratio in groundwater samples.

Table A.2. Total (particulate + dissolved) chemical composition of groundwater samples (July 5-8, 2016).

Table A.3. X-ray diffraction (XRD) analysis of five groundwater samples' residues (W3, W6, W7, W8 and B1: Fig. A.1.) and the new PTFE filter. The angle range and time measurements are different.

Table A.4. Pb isotopic ratios and contents in six grain-size categories and bulk from two surface soils.

Table A.5. The rare earth element concentration in total (particulate + dissolved) and dissolved components in groundwater samples (July 5-8, 2016).

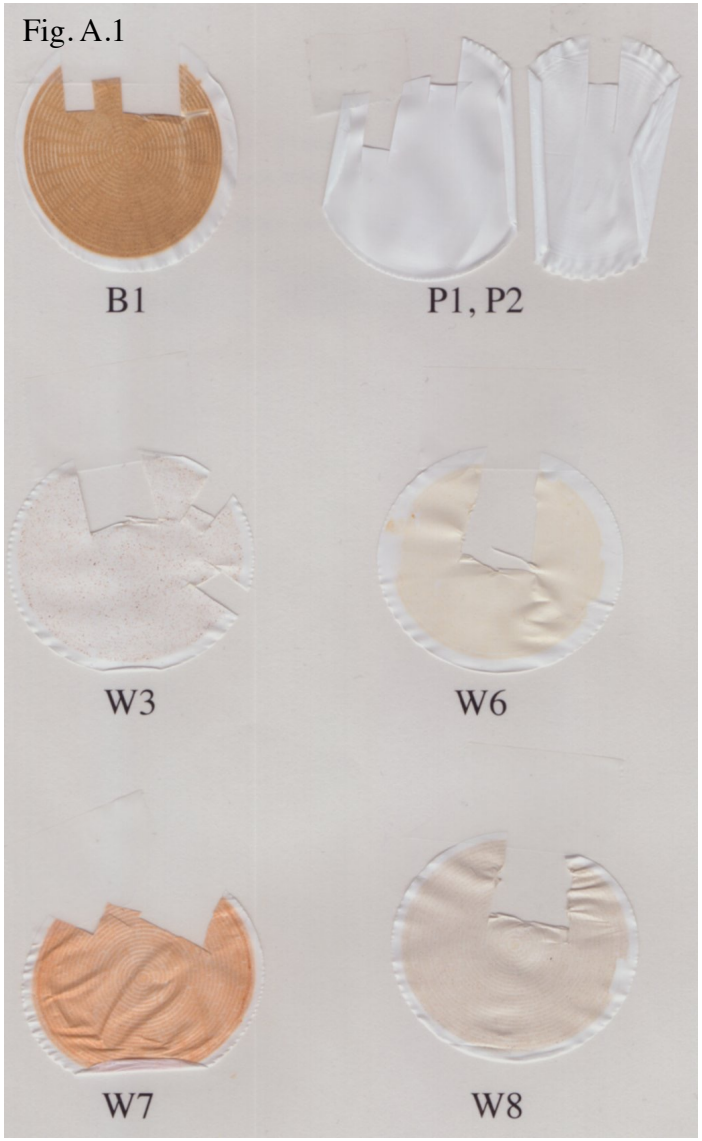

Fig. A.1. Picture of the groundwater samples" residue on the filter.

Fig. A.2. Pictures of the ground surface of a site on the tailing hill. The footprints in the picture replace the scale of the picture.

Table A.1. Dissolved (< 0.45 μm) minor element concentration and the total-Pb isotopic ratio in groundwater sample

Sample symbol	Minor cation concentration (μg/L) in dissolved component									Sample symbol	Total (particulate + dissolved) Pb isotope	
	Pb[&]	± S.D.[&]	Pb	Zn	Cu	Cd	Mn	Fe	Sb		$^{206}Pb/^{207}Pb$[&]	$^{208}Pb/^{206}Pb$[&]
P1	2.70	0.06	2.60	72.1	3.0	1.7	0.0	2.0	12.5	P1	1.1447 ± 0.0036	2.1360 ± 0.0060
P2	1.17	0.02	1.10	1096	0.8	2.5	0.0	3.4	1.2	P2	1.1457 ± 0.0036	2.1359 ± 0.0068
P3	13.9	0.2	13.1	717	118.5	6.5	135	1.2	4.0	P3	1.1450 ± 0.0028	2.1345 ± 0.0035
										P3[%]	1.1456 ± 0.0033	2.1340 ± 0.006
B1	2.18	0.03	2.12	8506	12.7	17.8	567	1.6	0.3	B1	1.1451 ± 0.0035	2.1336 ± 0.0056
B2	0.01	0.00	0.012	20.5	6.6	0.3	127	1.3	0.3	B2	1.1467 ± 0.0023	2.1285 ± 0.0041
B3	2.81	0.03	2.61	427	2.7	1.5	2.5	1.7	0.5	B3	1.1447 ± 0.0031	2.1363 ± 0.0044
W1	0.01	0.00	0.020	24.7	0.1	0.2	0.0	0.0	0.1			
W2	0.02	0.00	0.020	91.4	0.3	0.4	0.0	0.0	0.9	W2	1.1464 ± 0.0047	2.1361 ± 0.0080
W3	0.01	0.00	0.011	29.3	0.6	0.1	1185	0.7	0.4	W3	1.1471 ± 0.0033	2.1319 ± 0.0059
W4	0.06	0.00	0.013	0.7	0.3	0.0	0.1	0.2	0.2	W4	1.1458 ± 0.0035	2.1319 ± 0.0056
W5	0.03	0.00	0.027	0.5	0.1	0.0	0.0	0.7	0.1	W5	1.1460 ± 0.0039	2.1302 ± 0.0073
W6	0.01	0.00	0.009	0.8	0.1	0.0	0.0	0.0	0.2	W6	1.1477 ± 0.0026	2.1292 ± 0.0059
W7^	0.01	0.00	0.011	0.6	0.1	0.0	0.0	1.6	0.1	W7^	1.1611 ± 0.0030	2.1115 ± 0.0070
W8	0.02	0.00	0.016	0.7	0.5	0.0	0.0	3.1	0.3	W8	1.1457 ± 0.0035	2.1336 ± 0.0056
W9	0.02	0.00	0.010	0.6	0.0	0.0	0.0	0.4	0.0			
W10	0.01	0.00	0.017	0.6	0.0	0.0	0.0	2.4	0.1			
W11	0.02	0.00	0.026	4.8	0.2	0.1	0.0	0.7	0.1	W11	1.1429 ± 0.0039	2.1301 ± 0.0115
W12	0.01	0.00	0.013	0.6	0.1	0.0	0.0	1.6	0.1			
W13	0.01	0.00	0.016	31.4	0.2	0.0	18.3	1.7	0.3			
W14	0.04	0.00	0.028	5.2	0.2	0.0	5.8	1.0	0.1			
W15	0.01	0.00	0.006	0.8	0.2	0.0	0.4	2.4	0.1	W15	1.1719 ± 0.0038	2.0949 ± 0.0109
W16	0.03	0.00	0.040	86.0	0.2	0.5	0.0	0.8	0.1	W16	1.1464 ± 0.0024	2.1342 ± 0.0064
W17	0.01	0.00	0.009	23.5	0.2	0.0	0.0	2.9	0.0	W17	1.1463 ± 0.0044	2.1323 ± 0.0064
T1	0.01	0.00	0.015	0.4	1.3	0.0	0.0	2.1	0.0			
F1	0.01	0.00	0.017	0.0	0.2	0.0	0.0	2.6	0.1			
F2	0.02	0.00	0.026	2.0	3.5	0.1	0.2	2.7	0.2			
D1	0.02	0.00	0.011	1.9	0.0	0.0	0.0	0.0	0.0			
D2	0.02	0.00	0.014	0.5	0.0	0.0	7.0	0.0	0.1			

^: Disinfectant was added into the well a few days before the water sampling.

&: Master thesis (2017) by Nakano; %: Only this data is in dissolved component.

Table A.2.Total (particulate + dissolved) chemical composition of groundwater samples (July 5-8, 2016) .

Sample symbol	Major cation concentration (mg/L) by ICP-AES						Minor cation concentration (μg/L) by ICP-MS								
	Fe	Al	Mn	Na	Mg	Ca	Pb[&]	± SD[&]	Pb	Zn	Cu	Cd	Mn	Fe	Sb
P1	0.03	0.043	0.009	11.8	63.2	115.5	106	11	102	529	8.8	2.2	16	35	11.7
P2	*	0.035	0.005	17.6	87.4	48.3	41.0	3.3	40.9	1808	2.6	2.8	10	17	1.2
P3	0.13	0.143	0.193	16.4	64.5	140.0	152	8	161	1331	223	6.7	160	128	4
B1	8.97	17.5	3.93	13.2	76.5	126.8	2029	130	2177	12552	197	29.9	3200	8592	4
B2	0.99	0.182	1.91	32.5	72.1	70.0	47.1	3.4	56.4	502	126	0.6	1579	949	1
B3	0.10	0.096	0.012	10.4	63.2	108.3	86.2	4.6	91.2	674	7.4	1.5	11	89	2
W1	0.07	0.136	*	25.5	57.9	74.2	1.7	0.2	1.6	102	0.3	0.2	4	72	0.2
W2	0.05	0.229	0.012	22.5	67.5	60.0	5.1	0.0	5.8	294	0.6	0.5	26	93	1.7
W3	2.94	0.295	2.39	33.3	59.4	60.0	14.3	1.2	15.0	73	1.9	0.2	2414	2939	0.7
W4	0.52	0.474	1.073	50.2	61.3	41.6	6.6	0.8	7.4	28	1.3	0.1	1043	498	0.6
W5	0.06	0.076	*	29.6	76.5	54.7	6.1	0.4	6.1	12	0.7	0.0	7	74	0.1
W6	1.54	1.711	0.100	39.4	61.7	61.3	11.8	1.0	12.9	24	2.2	0.1	110	1470	0.3
W7^	12.61	6.12	0.088	23.4	50.0	27.0	19.0	0.1	19.4	33	6.8	0.0	94	11524	0.6
W8	1.18	1.137	0.245	20.6	49.2	10.2	75.0	9.0	72.8	126	5.3	0.3	266	1218	0.6
W9	0.22	0.127	*	24.9	36.8	55.4	2.5	0.2	2.4	5	0.4	0.0	8	261	0.1
W10	1.46	1.010	0.016	15.3	28.7	38.5	1.6	0.2	1.6	6	1.8	0.0	24	1524	0
W11	0.18	0.315	0.029	25.5	143.0	94.0	5.8	0.8	5.8	49	0.7	0.1	31	180	0
W12	0.03	0.079	0.007	26.0	56.6	54.5	2.3	0.2	2.4	11	0.4	0.0	15	57	0
W13	5.25	0.074	0.011	39.4	72.0	52.1	3.0	0.2	3.2	109	4.6	0.0	20	5162	1
W14	0.76	1.040	*	10.2	1.9	1.2	2.8	0.3	2.8	14	1.9	0.0	12	860	0
W15	1.79	2.07	0.378	9.2	6.6	13.3	5.1	0.8	5.0	9	3.9	0.0	350	1762	0
W16	0.16	0.197	0.007	9.1	47.3	76.8	5.9	0.8	5.7	248	0.5	0.5	9	162	0
W17	0.53	0.870	0.071	15.9	43.5	69.9	15.7	1.0	15.1	74	2.3	0.0	58	478	0
T1	0.06	0.054	0.013	11.0	37.6	34.9	0.93	0.16	0.89	14	2.4	0.0	10	71	0
F1	*	0.037	*	5.7	42.6	48.5	0.13	0.02	0.11	12	0.3	0.1	0	0	0.1
F2	*	0.030	*	5.1	43.2	68.9	0.42	0.05	0.42	31	4.4	0.1	0	1	0.1
D1	0.05	0.02*	*	8.7	41.4	32.5	---	---	1.75	9	0.0	0.0	0	81	0
D2	0.25	0.053	*	10.6	23.9	50.0	---	---	0.25	62	0.2	0.0	6	150	0

^: Disinfectant was added into the well a few days before the water sampling; [&]: Master thesis (2017) by Nakano

*: BDL: below determination limit

Table A.3. X-ray diffraction (XRD) analysis of five groundwater samples' residues (W3, W6, W7, W8 and B1: Fig. A.1.) and the new PTFE filter. The angle range and time measurements are different.

New PTFE filter			W3			W6			W8			W7			B1			Mineral identification
2θ (°)	d (Å)	Intensity (cps)	2θ (°)	d (Å)	Intensity (cps)	2θ (°)	d (Å)	Intensity (cps)	2θ (°)	d (Å)	Intensity (cps)	2θ (°)	d (Å)	Intensity (cps)	2θ (°)	d (Å)	Intensity (cps)	
4.63	19.1	54612				4.55	19.39	57168							4.25	20.773	21588	unused PTFE filter?
									5.02	17.603	9206				4.95	17.847	17408	
						8.98	9.84	9391	9.01	9.807	4246	9.00	9.820	18030	8.81	10.027	2258	Illite-2M2 (NR) (00-043-0685): 0 0 2
						12.37	7.15	8931	12.30	7.189	3521	12.46	7.096	9243	12.31	7.185	43873	Kaolinite-1Ad (00-058-2006): 0 0 1
16.44	5.389	11430	16.48	5.374	46582	16.46	5.38	89055	16.47	5.376	63492	16.43	5.392	9964	16.28	5.441	60717	unused PTFE filter?
18.20	4.870	750010	18.22	4.866	1415933	18.19	4.87	1970367	18.22	4.865	1830181	18.21	4.867	1087337	18.03	4.916	1197364	Teflon PFA (00-070-1340): 1 0 0
												20.99	4.228	5324				Quartz, syn: 1 0 0,Illite-2M2 (NR): 2 0 -2,Illite-1M (NR): 1 1 -1
22.72	3.910	204934	22.75	3.905	244126	22.73	3.91	201778	22.75	3.905	250549	22.74	3.908	168693	22.59	3.932	86115	Teflon PFA: 1 1 0
															24.03	3.700	488	Dolomite (00-036-0426): 0 1 2
															24.85	3.581	4835	Kaolinite-1Ad: 0 0 1
						24.99	3.56	1009							25.06	3.551	4013	Anhydrite ?; Illite-2M2 (NR): 1 1 -4 ?
						26.74	3.33	2348	26.79	3.326	651	26.78	3.326	28145	26.62	3.346	4006	Quartz, syn: 0 1 1,Illite-2M2 (NR): 0 0 6
						26.89	3.31	5474	26.92	3.310	2863	26.91	3.310	15650	26.79	3.325	3127	Illite-1M (NR): 0 0 3; Goethite: 1 2 0
												27.57	3.233	18813	27.41	3.251	1578	Quartz, syn (01-085-0794): 1 0 1
															27.88	3.197	348	Illite-2M2 (NR): 1 1 4
			28.71	3.107	1365	28.66	3.11	3156	28.66	3.112	676				28.49	3.130	1900	Montmorillonite-15A (00-013-0135): 0 0 5 ?
31.05	2.878	816													30.94	2.887	27994	Dolomite: 1 0 4 ?
31.73	2.818	20941	31.73	2.818	41494	31.70	2.82	49335	31.73	2.817	47749	31.73	2.818	32603	31.54	2.835	30198	unused PTFE filter ?
															33.53	2.670	3431	Dolomite: 0 0 6
															34.89	2.569	1222	Illite-2M2 (NR): 0 2 1,Illite-1M (NR): 1 3 -1,Mnt.-15A: 1 1 0
			35.30	2.541	1946										35.29	2.541	906	Dolomite: 0 1 5 ?
36.78	2.442	13068	36.77	2.442	28058	36.74	2.44	32077	36.77	2.442	28205	36.74	2.444	24169	36.56	2.456	17763	Teflon PFA: 2 0 0
												37.19	2.416	2632	37.34	2.406	735	Quartz, syn /Dolomite: 1 1 0
															37.74	2.382	186	Illite-2M2 (NR): 3 1 2,Dolomite: 1 1 0,Kaolinite-1Ad: 0 0 3
															38.53	2.335	230	Kaolinite-1Ad: 2 0 -2
															39.20	2.296	97	?
						39.61	2.27	1992	39.58	2.275	1559	39.60	2.274	1163	39.44	2.283	123	Muscovite-2M1 1 1 7 ?; Quartz, syn: 1 0 2
															40.27	2.238	670	Montmorillonite-15A: 2 0 0, Quartz, syn: 1 1 1
															41.11	2.194	2373	Dolomite: 1 1 3
												42.58	2.121	577				Quartz, syn ?
			43.45	2.081	291													?
															44.92	2.016	1204	Dolomite: 2 0 2
						45.49	1.99	2461	45.53	1.991	1771	45.49	1.992	8013	45.41	1.996	1996	Illite-1M (NR): 0 0 5,Kaolinite-1Ad: 2 0 -3
						46.53	1.95	1586							46.52	1.950	2018	?
												48.25	1.885	5057				Illite-1M (NR) (00-029-1496): 2 2 2
49.21	1.850	3971	49.27	1.848	9390	49.26	1.85	9808	49.29	1.847	9171	49.25	1.849	7851	49.08	1.855	7021	Teflon PFA: 2 1 0
												50.27	1.813	1718	50.10	1.819	251	Quartz, syn: 1 1 2
															50.53	1.805	4001	Quartz, syn: 0 0 3,Dolomite: 0 1 8
															51.07	1.787	2792	Dolomite: 1 1 6
															51.29	1.780	660	Dolomite: 0 0 9
			52.64	1.737	320													?
															54.22	1.690	690	portlandite ?
												54.98	1.669	742	54.84	1.673	160	Illite-2M2 (NR): 2 0 10,Montmorillonite-15A: 2 1 0
															55.23	1.662	1063	Muscovite-2M1 (00-058-2034): 2 0 -10 ?
56.42	1.630	4480	56.39	1.630	9263	56.37	1.63	10261	56.40	1.630	9071	56.43	1.629	7512	56.19	1.636	6503	Teflon PFA: 3 0 0
			57.57	1.600	726	57.87	1.59	5666										?
															58.90	1.567	104	Dolomite: 2 1 1
															59.82	1.545	691	Illite-1M (NR): 1 5 -3,Dolomite: 1 2 2
												60.09	1.539	1089				Quartz, syn 1 2 1 ?
66.07	1.413	2043	66.08	1.413	5751	66.12	1.41	4589	66.10	1.412	5096	66.16	1.411	3025				Teflon PFA: 2 2 0
												67.87	1.380	865				?
			68.28	1.373	152							68.27	1.373	1446				Goethite (00-029-0713): 3 3 0 ?
69.05	1.359	1750	69.12	1.358	4272	69.14	1.36	5332	69.17	1.357	5364	69.22	1.356	4759				Teflon PFA: 3 1 0
												75.80	1.254	590				Muscovite-2M1 ?

Table A4. Pb isotopic ratios and contents in six grain-size categories and bulk from two surface soils.

Sample symbol	grain size fraction (μm)	Pb (mg/kg)	206 Pb/ 207 Pb		208 Pb/ 206 Pb	
X S 14° 28'07 E 28° 26'05 1185 m	1000–2000	11563	1.1481 ±	0.0031	2.1307 ±	0.0050
	500–1000	10733	1.1456 ±	0.0016	2.1347 ±	0.0036
	300–500	3500	1.1437 ±	0.0017	2.1346 ±	0.0045
	100–300	2443	1.1436 ±	0.0018	2.1339 ±	0.0043
	53–100	2370	1.1444 ±	0.0016	2.1346 ±	0.0044
	< 53 μm	2319	1.1436 ±	0.0031	2.1334 ±	0.0071
	Bulk	2708	1.1454 ±	0.0022	2.1323 ±	0.0009
Y S 14° 26'30" E 28° 26'31' 1191 m	1000–2000	26	1.1776 ±	0.0021	2.0815 ±	0.0049
	500–1000	51	1.1591 ±	0.0024	2.1117 ±	0.0051
	300–500	88	1.1554 ±	0.0026	2.1144 ±	0.0073
	100–300	188	1.149 ±	0.0028	2.1284 ±	0.0078
	53–100	244	1.1498 ±	0.0029	2.1301 ±	0.0101
	< 53 μm	397	1.1478 ±	0.0015	2.1283 ±	0.0036
	Bulk	251	1.1500 ±	0.0027	2.1255 ±	0.0073
Kabwe PbS	Kamona et al. (1999)		1.1454 ±	0.0012	2.1342 ±	0.0027

Table A5. The rare earth element concentration in total (particulate + dissolved) and dissolved components in groundwater samples (July 5-8, 2016) . Table A4

Sample symbol	REE patterns of total component			ΣREE+Y (μg/L)	The rare earth element concentration (ng/L) in total (Particulate + Dissolved) components															
	La/Yb (± SD)		Ce/Ce* (± SD)	Eu/Eu*		Y	(± SD)	La	(± SD)	Ce	(± SD)	Pr	(± SD)	Nd	(± SD)	Sm	(± SD)	Eu	(± SD)	Gd	(± SD)	Tb
P1	10.4 ±	2.0	0.70 ± 0.14	0.64	0.24	60	6	35	3	55	4	9.7	1.7	45	4	8.7	1.5	1.5	0.5	5.7	0.7	0.88
P2	4.0 ±	1.0	0.52 ± 0.12	0.80	0.17	77	8	19	1	20	2	4.4	0.9	20	3	3.7	2.0	1.2	0.9	5.7	1.6	0.84
P3	11.3 ±	2.1	0.99 ± 0.08	0.68	0.47	90	7	68	3	145	5	17.5	1.2	74	5	16.4	4.9	3.8	0.4	17.7	1.1	2.67
B1	14.7 ±	1.6	0.46 ± 0.01	0.62	51.0	9100	104	10455	121	10034	77	2496.8	22.8	10520	116	1998.1	50.6	403.6	8.3	1990.7	23.6	277.42
B2	95.2 ±	19.1	0.45 ± 0.01	0.63	5.95	587	24	2147	18	1462	15	270.9	5.4	1034	36	132.6	8.4	27.2	1.8	132.9	5.8	13.06
B3	10.0 ±	0.7	0.61 ± 0.06	0.63	0.56	171	21	83	3	106	6	20.1	1.5	90	8	17.8	3.3	3.8	0.9	19.7	2.3	2.50
W1	17.5 ±	3.0	0.22 ± 0.01	0.70	0.91	239	9	198	6	89	4	46.7	2.1	198	6	28.3	5.9	7.5	1.6	38.4	7.2	4.50
W2	14.9 ±	2.6	0.21 ± 0.01	0.65	1.30	299	19	287	3	128	5	69.8	3.5	311	16	53.5	6.9	10.9	1.4	49.4	2.7	6.34
W3	78.6 ±	6.8	0.45 ± 0.02	0.73	4.27	324	12	1250	13	1077	8	251.3	9.3	986	29	136.7	10.5	28.7	3.7	105.4	4.1	10.15
W4	62.0 ±	12.8	0.46 ± 0.01	0.68	2.81	234	8	835	11	700	12	154.2	1.4	631	32	83.4	9.0	17.3	1.2	73.3	6.3	6.97
W5	46.1 ±	5.5	0.33 ± 0.01	0.79	1.55	184	9	415	6	282	4	94.1	1.8	399	27	56.9	4.6	13.5	1.1	48.2	3.8	4.59
W6	67.0 ±	2.9	0.40 ± 0.01	0.64	13.5	730	18	3705	38	3158	32	917.6	19.8	3599	89	544.1	29.1	92.0	2.8	356.6	6.0	37.52
W7^	56.8 ±	9.3	2.12 ± 0.04	0.59	33.0	979	21	4864	19	20357	108	1045.4	17.3	4139	57	594.2	19.7	99.3	2.6	444.3	15.3	44.44
W8	46.6 ±	10.6	0.98 ± 0.03	0.65	7.93	525	23	1714	18	3250	37	355.4	7.5	1435	14	224.0	23.8	42.2	5.1	175.0	10.5	18.49
W9	34.7 ±	11.2	0.81 ± 0.08	0.72	0.77	59	7	174	4	272	9	35.8	3.2	146	11	25.4	7.9	5.4	1.8	20.5	3.3	2.58
W10	56.1 ±	13.6	0.54 ± 0.01	0.56	10.2	579	19	2582	25	2890	19	614.3	11.0	2449	39	418.1	15.1	65.4	4.9	305.8	7.0	30.10
W11	32.0 ±	10.8	0.78 ± 0.06	0.67	1.37	121	7	297	9	470	9	66.8	4.4	272	21	41.4	4.4	8.3	2.6	34.9	3.7	4.25
W12	56.3 ±	6.2	0.22 ± 0.02	0.69	1.31	126	13	419	8	181	3	86.6	5.9	359	7	50.9	7.4	9.9	1.8	37.8	5.2	3.67
W13	108.2 ±	5.0	0.07 ± 0.003	0.68	2.69	272	13	1084	13	127	4	189.2	6.6	756	15	96.2	14.1	18.9	1.2	75.8	6.0	6.68
W14	19.0 ±	10.2	0.44 ± 0.01	0.64	7.41	729	29	1672	22	1611	12	435.7	9.9	1733	64	358.2	9.3	70.5	4.2	313.0	9.5	41.10
W15	40.0 ±	4.1	1.07 ± 0.02	0.59	19.3	988	15	3617	38	8328	61	923.8	13.2	3673	35	621.0	13.5	105.3	4.9	483.3	23.5	52.35
W16	14.0 ±	0.5	0.47 ± 0.02	0.49	1.68	363	12	294	5	309	3	82.6	3.7	353	13	61.9	9.2	10.9	1.8	75.0	4.6	8.62
W17	21.4 ±	6.3	0.62 ± 0.05	0.69	2.39	277	21	498	14	647	13	121.7	8.8	521	18	91.1	6.0	19.2	1.2	78.9	8.8	9.97
T1	12.1 ±	0.9	0.38 ± 0.05	0.53	0.48	94	11	94	7	84	3.5	28.2	2.7	111	9	15.4	5.1	3.1	0.8	20.3	3.3	2.11
F1	4.4 ±	1.1	0.35 ± 0.13	0.55	0.24	127	3	25	2	17	1	5.4	1.9	26	3	6.8	3.4	1.3	1.1	7.2	2.8	1.25
F2	5.1 ±	0.5	1.19 ± 0.24	0.57	0.21	83	5	17	1	57	3	5.8	0.9	20	2	4.2	2.5	0.9	0.4	5.8	1.7	0.75
D1	13.9 ±	3.4	0.13 ± 0.05	0.54	0.79	221	41	166	28	48	1	42.3	7.9	186	39	27.0	6.2	5.2	1.5	32.3	7.0	3.95
D2	6.8 ±	0.7	0.62 ± 0.15	0.32	0.13	32	4	21	2	29	3	5.7	1.2	21	5	4.0	2.0	0.5	0.5	5.5	1.7	0.61

Chondrite values for normalizing and standard sedimentary compositions (mg/I	Y	La	Ce	Pr	Nd	Sm	Eu	Gd	Tb
Evensen et al. (1978); Taylor and McLennan (1985): Average CI:	2.1	0.367	0.957	0.137	0.711	0.231	0.087	0.306	0.058
Gromet et al. (1984): North American shale composite (NASC):		31.1	67.0		30.4	5.98	1.25	5.50	0.850
IcLennan (1989); Post-Archaean average Australian sedimentary rock (PAAS):	27.0	38.2	79.6	8.83	33.9	5.55	1.08	4.66	0.774
Average upper continental crust (Taylor and McLennan, 1981):	22.0	30.0	64.0	7.10	26.0	4.50	0.88	3.80	0.640

(Continued)

The rare earth element concentration (ng/L) in total (Particulate + Dissolved) components													Particulate/Total conponent ratio (%)						Ce/Ce* (La-Ce-Nd)		
(± SD)	Dy	(± SD)	Ho	(± SD)	Er	(± SD)	Tm	(± SD)	Yb	(± SD)	Lu	(± SD)		∑REE+Y	Y	La	Ce	Y	(± SD)	particulate	Dissolved	La
0.19	6.7	2.1	1.4	0.4	3.6	1.2	0.5	0.2	3.4	0.8	0.5	0.1	**P1**	86	75	88	93	15.0	2.3	0.324	0.301 ± 0.096	4.1
0.36	5.7	0.8	1.5	0.3	4.2	1.1	0.5	0.3	4.7	0.8	0.9	0.4	**P2**	71	69	61	57	24.1	2.2	0.691	0.443 ± 0.067	7.4
0.35	14.8	0.7	2.6	0.6	7.1	0.7	1.1	0.4	6.0	1.2	0.7	0.6	**P3**	88	73	87	96	24.0	1.9	0.507	0.806 ± 0.212	9.0
4.42	1620.9	17.6	319.8	7.6	877.9	6.9	121.8	2.5	709.9	20.2	108.9	4.9	**B1**	100	100	100	100	5.6	0.5	0.215	0.080 ± 0.006	11.9
1.74	66.8	5.1	12.7	0.2	32.9	3.6	3.8	0.3	22.5	2.4	3.3	0.9	**B2**	99	97	99	100	19.5	1.1	0.207	0.057 ± 0.009	14.8
0.51	16.6	3.0	3.4	0.4	11.7	1.0	1.6	0.4	8.3	1.5	1.1	0.4	**B3**	88	81	88	96	32.3	3.8	0.446	1.208 ± 0.828	10.3
0.57	26.5	2.4	5.5	0.8	15.8	3.0	1.8	0.5	11.3	2.8	1.7	0.3	**W1**	73	59	78	91	99.0	3.8	0.440	0.197 ± 0.058	43.8
1.02	37.7	3.4	7.5	0.7	18.0	2.1	2.9	0.5	19.2	3.3	2.5	0.5	**W2**	87	77	90	97	67.4	3.4	0.329	0.108 ± 0.004	28.9
0.68	50.4	6.7	8.7	0.8	20.8	2.5	2.6	0.8	15.9	2.7	2.6	0.9	**W3**	100	100	100	99	1.3	0.2	0.411	0.302 ± 0.019	5.0
1.29	35.3	4.6	6.0	0.9	14.4	0.9	2.4	0.4	13.5	1.2	1.9	0.7	**W4**	99	97	99	100	6.8	0.9	2.112	0.440 ± 0.135	5.6
0.64	25.0	2.6	4.6	0.8	11.9	3.0	1.1	0.2	9.0	1.9	1.4	0.3	**W5**	73	53	72	91	85.7	7.3	1.375	0.177 ± 0.028	114.7
2.32	167.3	8.0	28.0	1.3	70.5	4.0	9.0	0.8	55.3	6.5	9.2	1.3	**W6**	99	95	99	99	34.5	4.6	0.962	0.879 ± 0.172	43.7
1.21	209.3	10.2	35.0	2.2	96.0	6.2	12.4	2.0	85.7	3.6	12.6	1.1	**W7***	100	100	100	100	0.7	0.5	0.791	0.273 ± 0.083	5.2
0.65	84.5	6.3	16.4	0.4	43.8	5.9	5.9	0.6	36.8	2.9	5.6	1.1	**W8**	100	100	100	100	2.1	1.3	0.545	0.039 ± 0.004	6.2
0.27	12.9	1.8	3.0	0.4	5.5	1.6	0.5	0.2	5.0	1.1	0.7	0.3	**W9**	98	95	98	99	3.0	1.5	0.132	0.059 ± 0.006	4.3
1.66	134.2	7.7	21.9	1.2	56.1	1.8	7.3	1.1	46.0	3.4	7.4	0.9	**W10**	97	91	97	100	51.6	3.4	0.780	0.155 ± 0.015	84.6
0.97	20.6	2.4	4.2	0.6	11.7	1.9	1.5	0.5	9.3	1.7	1.5	0.5	**W11**	88	67	86	97	39.5	3.3	0.217	0.123 ± 0.004	41.6
1.01	19.0	2.6	3.1	0.2	8.5	1.6	1.2	0.4	7.4	2.5	0.8	0.2	**W12**	79	59	81	89	51.4	1.7	0.063	0.909 ± 0.191	78.4
0.96	32.4	5.0	7.0	1.0	16.9	2.7	1.7	0.3	10.0	1.1	1.6	0.3	**W13**	100	100	100	97	1.3	0.4	0.455	0.414 ± 0.053	2.8
2.96	209.1	7.1	35.0	2.6	91.8	3.2	12.6	1.1	88.2	3.9	13.1	2.1	**W14**	99	98	99	99	16.2	1.7	0.659	0.539 ± 0.204	10.8
1.15	244.1	5.2	40.2	1.3	107.4	4.0	15.1	1.1	90.3	3.9	13.2	1.9	**W15$**	100	100	100	100	3.2	0.8	1.095	0.576 ± 0.038	8.3
0.73	55.2	5.0	10.9	1.4	27.6	3.3	3.6	0.7	20.9	2.1	3.8	0.5	**W16**	94	87	95	99	46.5	3.4	0.474	0.106 ± 0.012	14.4
1.50	59.5	4.8	10.1	1.0	27.6	4.5	4.4	0.4	23.2	1.5	3.6	0.7	**W17**	100	100	100	99	0.6	0.4	0.458	0.201 ± 0.036	2.1
0.52	11.8	2.0	2.4	0.5	6.3	0.9	1.1	0.4	7.8	2.3	0.9	0.3	**T2**	86	71	90	96	27.0	5.1	0.415	0.196 ± 0.041	9.7
0.32	8.4	1.1	1.6	0.5	6.2	1.2	0.6	0.2	5.7	1.3	0.7	0.3	**F1**	91	90	89	90	12.1	2.1	0.994	0.350 ± 0.061	2.8
0.40	6.0	2.1	1.3	0.6	4.2	1.5	0.8	0.5	3.3	0.5	0.4	0.4	**F2**	64	46	61	95	45.3	2.1	0.599	0.173 ± 0.050	6.6
0.89	25.2	4.6	5.3	1.2	14.1	3.4	1.8	0.5	12.0	2.9	1.6	0.7	**D1**	67	51	68	87	107.6	2.1	0.612	0.991 ± 0.470	52.6
0.30	4.5	0.8	1.1	0.4	2.8	0.8	0.5	0.2	3.1	1.7	0.7	0.3	**D2**	98	99	97	97	0.4	0.2	0.404	0.158 ± 0.016	0.7

	Dy	Ho	Er	Tm	Yb	Lu
	0.381	0.085	0.249	0.036	0.248	0.038
	5.54		3.28		3.11	0.456
	4.68	0.991	2.85	0.405	2.82	0.433
	3.50	0.800	2.30	0.330	2.20	0.320

W1–W17				
Avg.	93.2	86.9	93.7	97.5

Table A4 (Continued)

Rare earth element concentration (ng/L) in dissolved component																										
(± SD)	Ce	(± SD)	Pr	(± SD)	Nd	(± SD)	Sm	(± SD)	Eu	(± SD	Gd	(± SD)	Tb	(± SD)	Dy	(± SD)	Ho	(± SD)	Er	(± SD)	Tm	(± SD)	Yb	(± SD)	Lu	(± SD)	ΣREE+Y	(ng/L)
0.2	4.0	0.6	1.0	0.5	4.9	0.5	0.42	0.48	0.60	0.11	0.57	0.27	0.12	0.05	1.16	0.41	0.27	0.08	1.02	0.15	0.10	0.05	0.64	0.40	0.12	0.02	**P1**	34
0.5	8.8	0.6	0.9	0.0	2.6	1.4	0.83	1.03	0.69	0.43	0.36	0.22	0.12	0.08	1.07	0.20	0.29	0.05	1.65	0.32	0.15	0.05	0.41	0.09	0.05	0.06	**P2**	49
1.1	6.3	0.4	1.7	0.1	7.7	1.6	1.25	0.48	0.81	0.47	1.28	0.34	0.27	0.08	1.59	0.84	0.36	0.19	1.92	0.28	0.26	0.06	0.88	0.24	0.20	0.13	**P3**	58
0.6	4.3	0.5	1.6	0.4	7.6	1.9	0.49	0.52	0.89	0.13	0.46	0.31	0.07	0.06	0.23	0.13	0.13	0.03	0.31	0.24	0.02	0.02	0.08	0.12	0.00	0.00	**B1**	34
0.9	5.0	1.2	1.6	0.2	8.1	0.3	1.32	0.43	1.10	0.29	2.00	0.43	0.27	0.07	1.74	0.17	0.41	0.12	1.58	0.68	0.18	0.02	1.36	0.13	0.17	0.19	**B2**	59
1.0	3.9	0.8	2.3	0.6	11.5	3.2	0.76	0.21	0.84	0.25	1.64	0.34	0.20	0.10	2.35	0.30	0.51	0.13	2.04	0.28	0.15	0.03	0.46	0.16	0.00	0.00	**B3**	69
1.5	7.8	0.5	10.8	1.6	52.7	2.0	5.48	0.43	2.04	0.66	8.73	1.39	1.16	0.09	7.63	0.53	1.84	0.42	5.81	0.75	0.63	0.16	2.63	0.16	0.52	0.23	**W1**	251
1.2	3.7	0.6	6.8	0.5	34.9	3.7	4.58	1.25	1.10	0.30	4.42	1.51	0.53	0.02	4.15	0.95	1.34	0.30	3.96	0.39	0.36	0.08	1.34	0.25	0.11	0.06	**W2**	164
0.1	6.9	0.2	0.3	0.2	0.8	0.9	0.14	0.36	1.42	0.35	0.39	0.49	0.04	0.02	0.20	0.20	0.05	0.04	0.17	0.06	0.01	0.01	0.05	0.00	0.09	0.12	**W3**	17
0.9	2.0	0.4	0.9	0.4	3.9	0.9	0.49	0.32	1.34	0.31	0.36	0.06	0.05	0.03	0.61	0.09	0.12	0.07	0.56	0.13	0.12	0.04	1.00	0.04	0.20	0.08	**W4**	24
0.5	25.5	0.5	24.3	1.4	109.6	7.5	14.71	2.66	5.23	1.26	13.58	0.38	1.47	0.17	6.50	0.05	1.60	0.13	4.02	0.54	0.60	0.08	3.24	1.02	0.63	0.37	**W5**	412
2.2	27.1	0.6	8.3	0.7	41.4	3.7	5.34	1.04	3.99	0.21	4.56	0.81	0.44	0.06	3.10	0.57	0.92	0.24	2.58	1.06	0.33	0.04	1.62	0.24	0.16	0.09	**W6**	178
0.7	3.3	0.5	0.6	0.1	1.7	0.6	0.00	0.00	1.20	0.33	0.07	0.19	0.03	0.01	0.09	0.09	0.00	0.00	0.10	0.09	0.01	0.02	0.10	0.12	0.02	0.04	**W7***	13
0.8	8.0	0.5	0.6	0.3	2.1	0.6	0.21	0.32	3.50	0.74	0.25	0.12	0.05	0.00	0.38	0.05	0.03	0.03	0.13	0.15	0.06	0.03	0.41	0.16	0.16	0.09	**W8**	24
0.7	2.4	0.2	1.0	0.2	3.8	1.6	0.14	0.21	0.74	0.28	0.21	0.06	0.02	0.03	0.17	0.30	0.08	0.03	0.35	0.12	0.02	0.01	0.13	0.08	0.01	0.02	**W9**	16
1.1	7.0	0.8	18.0	1.7	88.5	7.0	10.47	2.24	2.02	0.17	10.51	0.83	0.85	0.33	5.68	0.52	1.34	0.25	3.37	0.27	0.40	0.07	1.08	0.39	0.14	0.09	**W10**	286
1.5	12.8	1.2	8.1	1.2	36.3	1.7	5.62	1.68	1.42	0.33	4.70	0.06	0.73	0.04	3.80	0.13	1.15	0.20	3.54	0.94	0.40	0.04	1.47	0.09	0.36	0.11	**W11**	161
2.7	19.8	0.2	16.7	1.3	75.0	4.0	8.95	1.15	3.34	0.45	7.56	0.49	0.92	0.19	5.83	0.91	1.16	0.23	3.41	0.72	0.38	0.16	2.39	0.65	0.44	0.23	**W12**	276
0.3	3.3	0.5	0.2	0.1	0.6	0.1	0.07	0.24	2.06	0.32	0.07	0.11	0.00	0.00	0.09	0.09	0.01	0.01	0.02	0.03	0.00	0.00	0.08	0.09	0.01	0.02	**W13**	11
0.5	13.4	1.0	6.5	0.4	31.3	6.0	7.35	0.94	1.78	0.30	5.95	1.13	0.75	0.11	4.32	0.22	0.73	0.10	2.94	0.85	0.56	0.14	3.89	0.58	0.82	0.20	**W14**	107
0.3	11.3	0.5	2.5	0.3	11.9	0.8	2.71	0.12	1.44	0.49	1.43	0.43	0.14	0.05	0.96	0.31	0.16	0.00	0.31	0.13	0.08	0.06	0.46	0.24	0.22	0.06	**W15$**	45
1.0	3.6	0.4	3.8	0.4	20.5	0.7	2.29	1.15	0.94	0.55	2.28	0.86	0.38	0.06	3.33	0.35	0.98	0.14	2.89	0.32	0.37	0.07	1.36	0.41	0.14	0.06	**W16**	104
0.5	3.5	0.5	0.2	0.2	1.1	0.6	0.14	0.21	0.22	0.03	0.00	0.00	0.01	0.01	0.12	0.20	0.03	0.03	0.04	0.07	0.02	0.04	0.03	0.09	0.02	0.04	**W17**	8
1.2	3.6	0.1	2.2	0.2	13.3	1.1	1.60	0.75	1.06	0.17	1.82	0.43	0.25	0.08	2.17	0.69	0.58	0.17	1.54	0.23	0.18	0.04	0.52	0.28	0.10	0.04	**T2**	66
0.4	1.6	0.4	0.6	0.2	2.3	0.3	0.14	0.36	0.27	0.18	0.11	0.12	0.04	0.04	0.46	0.13	0.16	0.02	0.56	0.15	0.11	0.05	0.03	0.09	0.01	0.02	**F1**	21
0.4	2.7	0.3	1.8	0.1	8.6	1.2	1.11	0.64	0.51	0.19	1.57	0.57	0.31	0.10	2.52	0.69	0.50	0.14	2.46	0.37	0.35	0.13	1.03	0.53	0.14	0.02	**F2**	75
0.7	6.4	0.7	10.6	0.5	49.5	0.9	6.38	1.50	1.22	0.23	7.31	0.34	1.01	0.16	8.55	1.00	1.96	0.29	6.00	0.10	0.61	0.09	2.81	0.09	0.67	0.23	**D1**	263
0.1	0.8	0.2	0.0	0.1	0.7	0.2	0.00	0.00	0.03	0.03	0.00	0.00	0.01	0.01	0.14	0.13	0.01	0.01	0.23	0.12	0.01	0.01	0.00	0.00	0.00	0.00	**D2**	3

^: Disinfectant was added into the well a few days before the water sampling.